Modeling the urban circulation in the Salt Lake City area using the WRF urban canopy parameterization*

Thomas Nehrkorn†, John Henderson, Mark Leidner, Marikate Ellis,
Andrew Maher and Janusz Eluszkiewicz
Atmospheric and Environmental Research Inc., Lexington, MA 02421

1. Introduction

Historically, the primary motivation for conducting urban meteorology field programs, and for improving the modeling of atmospheric transport and dispersion (ATD) in urban areas, has been for air pollution applications, and for the accurate modeling of accidental releases of harmful materials. The work reported here was motivated by a slightly different application: the increasingly important need to monitor green house gas emissions.

Monitoring of current and modeling of future emissions of CO_2 from urban areas are important components of climate change research and monitoring. Accurate estimates of CO_2 emissions require a combination of approaches: using inventories of known anthropogenic and natural sources ("bottom-up" approach); analyzing flux measurements at selected sites; and combining concentration measurements with transport and dispersion computations to constrain prior estimates of sources ("top-down" approach). As part of a larger "top-down" effort to determine the feasibility of using ground-based sensors to identify trends in anthropogenic urban emissions over a range of time scales (from days to years), we have conducted simulations over the Salt Lake City (SLC) area with the Weather Research and Forecast (WRF, Skamarock and Klemp 2008) model. These simulations, when combined with a Lagrangian particle dispersion model (WRF-STILT, Lin et al. 2003; Nehrkorn et al. 2010) and emissions inventories (VULCAN, Gurney et al. 2009) allow the modeling of CO_2 concentrations that can be compared with *in situ* measurements.

A pre-requisite for successful modeling of these concentrations is the fidelity of the WRF simulation of the urban environment, the local and mesoscale circulations, and the atmospheric boundary layer in the SLC area. The Vertical Transport and Mixing (VTMX) field experiment dataset from 2000 provided the opportunity to assess the performance of the latest version of WRF in this environment, and to guide the selection of model configurations for this application. A series of sensitivity experiments was performed for two of the VTMX Intensive Observing Periods (IOPs). The WRF configurations were chosen to compare the performance of different PBL schemes with, and without, use of an urban canopy model (UCM) (see Section 2).

These simulations complement earlier modeling studies using VTMX data. For example, an intercomparison of different mesoscale model simulations (Zhong and Fast 2003) found that all three models examined (MM5, Meso-Eta, and RAMS) were generally successful at reproduc-

*Allwine-Doran Retrospective of the Special Symposium on Applications of Air Pollution Meteorology, January 2011

†AER, Inc, 131 Hartwell Avenue, Lexington, MA 02421; tnehrkor@aer.com

ing the important mesoscale circulation, but all had important short-comings in capturing the diurnal cycle of the near-surface temperature. That study examined the same IOPs (7 and 10) used in the present study. The performance of a high-resolution version of the COAMPS model with a multi-layer UCM was examined by Chin et al. (2005) for IOP 10. They found that including the UCM improved some aspects of the simulations (particularly winds), but not others (temperature). The experimental design for our WRF sensitivity experiments are described in the next section, followed by a description of the results in Section 3, and summary and conclusions in Section 4.

2. Experimental Design

a. *Selection of WRF configurations*

The Advanced Research version of WRF (ARW) was used for these experiments. A total of 4 nested domains, with resolutions down to 1.3 km, were centered over the SLC area (see Fig. 1). In the vertical, 41 levels were used, with 11 layers below 2 km. A summary of WRF configurations common to all WRF runs is shown in Table 1. The effect of varying the of the planetary boundary layer (PBL) parameterization and the urban surface were investigated by conducting the four sensitivity test runs summarized in Table 2. The two PBL schemes were selected as the most widely used representatives of a first-order (eddy diffusivity) turbulence scheme (YSU) that incorporates the effects of non-local mixing (hereafter, "Eddy"), and a higher-order (MYJ), turbulent kinetic energy based scheme (hereafter, "Turb"). Comparisons in the literature between these and other PBL schemes have been conducted for different locations and times of year, with varying results. For example, Otkin and Greenwald (2008) found insufficient vertical mixing, particularly for the MYJ scheme, in simulations over the North Atlantic, while Bowman (2009) noted too much mixing in simulations of the mountainous Pacific Northwest, regardless of the PBL scheme, in both MM5 and WRF. In summertime simulations over the Central US, Hu et al. (2010) attributed larger positive temperature and negative moisture biases in MYJ (compared to YSU) to an underestimate of vertical mixing caused by the lack of non-local mixing in the MYJ scheme.

For an accurate representation of the urban environment, it is necessary to incorporate interactions between the urban landscape (e.g., residential and commercial buildings of varying heights, paved surfaces) and the overlying atmosphere. While a detailed treatment of flow around invidual buildings is beyond the scope of what can be represented in a mesoscale model, bulk effects of the urban "canopy" (in analogy to vegetative canopies such as forests) can be represented in urban canopy models (UCMs). WRF includes two options for UCMs: one is a single-layer treatment chosen here, another is a multi-layer parameterization (BEP), which would require very high vertical resolution within the PBL, and which is only compatible with the Boulac second-order PBL scheme. An intercomparison of the WRF single and multi-layer UCMs within the COAMPS model for the New York City area (Holt and Pullen 2007) found no advantage of the added complexity and computational expense associated with the multi-layer scheme. A detailed description of the single-layer UCM is provided in Chen et al. (2010). Our experimental design includes two runs for each choice of the PBL scheme, one with, and one without, the single-layer urban canopy parameterization (UCM). (Hereafter, the suffix "-U" is added to the corresponding experiment name.) The two runs without the UCM were completed with WRF version 3.2. Runs with the UCM were completed with version 3.2.1, because the new version included improvements specifically for the UCM. In addition, the land-use data were refined for the UCM runs with high-resolution data that included 3 separate categories of urban land use (see the next section), rather than

the single urban category used by default. Initialization of the various UCM parameters was based on the default parameters established for the three-category urban land use types (Chen et al. 2010).

b. *Land-use datasets*

In order to take full advantage of the UCM's capabilities, it is important to incorporate high resolution urban land use data into the WRF model treatments where the UCM is applied. High resolution urban land use data allows the UCM to better represent fields such as urban geometry, skin temperatures of urban infrastructure, and friction velocity. To this end, a new 1-s resolution landuse dataset with three urban classifications (low and high intensity residential, and industrial or commercial) based on 2001 National Land Cover Data (NLCD 2001) was obtained from the Multi-Resolution Land Characteristics Consortium (MRLC). For the UCM simulations only, the land use index values of grid points (within the area covered by domain 4) was modified to one of the three urban categories where applicable. The resulting blended landuse dataset is denoted by "LU33", while the original landuse dataset is denoted by "LU24".

Fig. 2 and Fig. 3 display the urban land use categories of LU24 and LU33 respectively. Note that the main area of Salt Lake City itself is the high density urban area between 40.5 and 41.0 degrees North latitude. Comparison of the urban regions of LU24 and LU33 shows that the new LU33 dataset adds considerable detail to the definition and extent of the urban regions in domain 4, especially on the western side of Salt Lake City. This change in detail is best seen in Fig. 4 where the land use index difference is displayed.

While the differences in the land use maps are important in the innermost domain, d04, they are less significant in domains d01, d02 and d03 (not shown). In d01, the land use differences appear as only several pixels within the entire domain.

c. *VTMX data*

The VTMX was a multi-institutional campaign that was conducted in the vicinity of Salt Lake City during October 2000 (Doran et al. 2002) and provided the means for verifying upper air fields in the WRF treatments. The three rawinsondes and three radar wind profilers available for IOPs 7 and 10 are located at different sites throughout the Salt Lake Valley (Fig. 5). The rawinsondes (VX010, VX080, and VX120), located at the north end, center, and south end of the valley, respectively, provided profiles of wind, temperature, and humidity. Data frequency ranged from hourly up to every three to four hours.

The VTMX 915-MHz profilers are located at the center of the valley (VX070), on the eastern edge of the valley close to the Wasatch Mountain range (VX050), and at the mouth of a canyon (VX090). Data from the wind profiler operating in both high and low modes were used for verification. Low-mode data have finer resolution at low levels but a lower usable data ceiling, a consequence of a shorter pulse length and lower signal-to-noise ratio. High-mode data are available at higher altitudes, but with coarser vertical resolution. Consensus data from VX050 and VX090 were averaged over 50-60 minute intervals, while data from VX070 were averaged over 30 minutes according to the NCAR Improved Moment Algorithm (NIMA) in an attempt to improve data quality. Additionally, VX070 and VX090 were equipped with radio acoustic sounding systems (RASS) that return profiles of virtual temperature. However, the RASS data quality was questionable and was excluded from this analysis.

d. *Selection of Intensive Observing Periods*

A goal of the VTMX program (Doran et al. 2002) was to better understand the meteorological processes affecting transport and mixing in the

atmosphere, with a focus on the nocturnal stable periods and the morning and evening transition periods, especially in urban valley areas. It may be illustrative, therefore, in the current study to select IOPs characterized by substantially different large and small-scale flow patterns. Doran et al. (2002) grouped the IOPs into two categories based on the amount of modulation by the synoptic-scale flow on the smaller-scale drainage circulations. One IOP from each category has been selected for use in the current study. IOP 7, from 2200 UTC 17 October to 1600 UTC 18 October, was characterized by quiescent synoptic-scale flow until about 0500 local time, yet sufficient insolation thereafter such that robust valley and mountain breezes developed (Zhong and Fast 2003). In contrast, daytime cloud cover and southerly surface winds associated with the approach of a synoptic-scale trough during IOP 10, which was held from 2200 UTC 25 October to 1600 UTC 26 October, substantially reduced local effects.

3. Results

WRF forecasts are evaluated in this section to determine which model setup provides the best overall simulation of meteorological conditions, particularly for driving models of atmospheric transport and dispersion. The spatial pattern of differences between WRF model configurations are described in Section a. The WRF forecasts are then verified by comparing to regional observations including Mesowest surface observations (Section b, “Surface Station Verification”) and VTMX upper air observations (Section c, “Radiosonde and Profiler Verification”).

a. *Sensitivity to WRF configurations*

WRF forecasts are compared to each other in this section to identify spatial differences in near surface parameters important to atmospheric dispersion. Differences have been examined in (1) 2 m temperature, (2) the height of the planetary boundary layer, and (3) 10 m wind speed.

To set the stage for these results, recall that the meteorology of the boundary layer and urban environments are closely tied to the diurnal heating cycle. For example, the boundary layer height during the over night hours is often near zero, since, typically, the boundary layer collapses at night without solar heating of the surface. Therefore, differences in PBL height between the model configurations should be minimal at night, and more meaningful differences might be seen during the day, when the PBL depth is maintained by solar forcing. Another example: 2 m temperature during the over night hours is typically controlled by longwave cooling and local surface radiative characteristics. Therefore, differences in 2 m temperatures between the model configurations should be largest at night where the surface radiative properties have been redefined (LU24 to LU33; mostly urban and suburban areas). Whereas during the day, strong solar forcing at the surface and mixing in the boundary layer tend to homogenize the surface temperature more than at night and should result in smaller model-to-model differences.

Varying the treatment of the PBL and/or the urban canopy produces noticeable differences in the model results. Some of the differences can be attributed to slight changes from the WRF v3.2 to v3.2.1. Other differences are consistent with the use of different physical parameterizations, whose various effects can accumulate during the forecast to produce local, transient forecast differences. The most pronounced and repeatable differences are seen in the 2 m temperatures during the overnight hours. Fig. 6 and Fig. 7 show the differences in 2 m temperature between UCM and non-UCM forecasts after the overnight hours of October 17-18th (IOP7). Around the Salt Lake City area, the early morning temperatures are predominantly colder using the UCM, because large urban areas were converted to low intensity residential (category 33) from their prior, single ur-

ban classification (category 1; these grid points appear as light blue areas in Fig. 3). Low intensity residential areas will cool faster at night than the prior, single urban classification because the surface emissivity is higher. However, the highest intensity urban areas, which have been reclassified as high intensity residential or industrial/commercial in the LU33 classification, stay warmer at night than the prior, single urban classification. This can be seen as scattered positive differences (orange and red areas) in the Salt Lake City urban area (see Fig. 6. The positive differences are not as evident in Fig. 7, because, as will be shown later (cf. Fig. 14), the "Turb" PBL scheme produces overnight 2 m temperatures that are several degrees too warm compared to the "Eddy" PBL scheme, and even warmer still than observations. So in the case of the "Turb" PBL scheme, the UCM cools the nighttime near-surface temperatures more than when the "Eddy" PBL scheme is used, since there is a larger warm bias to correct.

In contrast to the differences in overnight temperatures, daytime temperature differences between UCM and non-UCM model configurations, forced by solar heating and homogenized by boundary layer mixing, are much smaller (less than 1 or 2 °C; see Fig. 8 and Fig. 9), regardless of PBL scheme.

The consistent positive temperature differences over the Great Salt Lake in the prior 4 figures are owing to differences between WRF v3.2 and v3.2.1, since these differences are not present in comparisons of Turb to Eddy or Turb-U to Eddy-U.

The differences in 10 m wind speed and PBL height are more difficult to characterize, since these differences are not stationary in space and are transients in the local flow over time scales of 1-3 hours. The PBL does collapse each night for all model configurations, and so the differences in PBL height between different model configurations are very small. But during the day, non-stationary, transient differences of up to a few hundred meters, both positve and negative, seem to be present across the 1.3 km grid. These differences move and evolve with the flow. Something very similar can be said for differences in 10 m wind speed with differences of 1-4 m s^{-1}, both positive and negative. Fig. 10 and Fig. 11 show snapshots of typical differences in PBL height and 10 m winds, respectively.

Differences are noted in all three parameters, 2 m temperature, PBL height and 10 m wind speed when comparing the results of different model configurations, but only the differences in 2 m temperature are stationary and clearly tied to use of the UCM/improved surface characterization (LU33). While differences are noted between the WRF forecasts that use YSU and MYJ PBL parameterizations, no consistent spatial pattern or diurnal cycle in the differences is evident.

b. *Surface Station Verification*

i. Time series Time series of temperature forecasts from the four WRF simulations were overlayed with observations from the VTMX mesonet surface stations. It was expected that forecast improvements would appear as increased temperature spread among the four forecasts, with perhaps clustering of the runs that used the UCM draw more closely towards the observed values. The ability to draw overarching conclusions was limited by the limited number of stations that passed the most rigorous quality control measures of the MesoWest dataset (fewer than ten), small number of IOP periods, and significant number of missing observations at some of the stations.

Overall, the daytime temperature forecasts were similar, especially during the morning hours when the nocturnal inversions dissipated and strong surface heating occurred. The most prominent feature in the verification plots is the improvement in nighttime temperature forecasts in urban areas by the two UCM simulations. This appears in Fig. 12a as increased

spread in the overnight temperature traces, with the Eddy-U and Turb-U simulations better simulating the strong surface-based inversion that formed. Fig. 12b shows the corresponding decrease in bias and rms associated with these two WRF simulations.

Outside the urban core, it was noted that the choice of PBL scheme was more important for the accuracy of the overnight temperature forecasts, though this observation is less robust across the set of rural stations and two IOPs. Fig. 13 demonstrates that the Eddy and Eddy-U simulations significantly better predicted overnight temperatures. It is possible that for this location, which is in a canyon amid complex topography during the quiescent IOP 7, the simulations that used the eddy diffusivity-based YSU PBL scheme better represented the localized drainage of cool air. Analysis of plots of wind speed and direction was inconclusive.

ii. Spatial Statistics In order to calculate spatial statistics using WRF-MET, only those MesoWest stations with data that underwent strong quality control measures are utilized (5-10 stations). Fig. 14 and Fig. 15 depict IOP 7 bias and root mean squared error respectively, while Fig. 16 and Fig. 17 depict IOP 10 bias and root mean squared error respectively. In these figures, blue colors indicate runs that have the “Eddy” PBL scheme (YSU), green colors indicate runs that have the “Turb” PBL scheme (MYJ), while light and dark colors correspond to UCM and non-UCM runs, respectively.

In the Fig. 14 temperature panel, the UCM treatments (light colors) have a smaller positive bias compared to the non-UCM treatments (dark colors), particularly during the evening and nighttime periods: 8-15 hrs and 24-30 hrs. This nocturnal difference is also reflected in the RMSE (Fig. 15). This statistical result confirms the spatial difference pattern shown in Fig. 6 and Fig. 7, and the individual station results shown in Fig. 12. In contrast, the non-UCM temperature bias is smaller for the synoptically disturbed IOP 10 (Fig. 16), and the cooler UCM-run temperatures result in negative biases of similar magnitude. As a result, the RMSE (Fig. 17) is virtually identical for all experiments.

The RMSE and bias for wind fields are similar for runs using the same PBL scheme (unlike what was seen for temperature): dark and light lines of the same color tend to group together in the wind speed, u-wind, and v-wind panels in Fig. 14, Fig. 15, Fig. 16, and Fig. 17. Overall, differences between the experiments are smaller for these fields than temperature, with only a slightly smaller bias and RMSE (most noticeable for wind speed) for the runs with the Eddy PBL scheme (YSU).

Error statistics for dewpoint temperature and relative humidity are virtually identical for all experiments. An interesting feature is that for IOP 7, there is a clear diurnal signal (nighttime underprediction of moisture), while for IOP 10 the moisture bias changes monotonically throughout the period reflecting errors in the synoptic trends during that time.

The spatial statistics suggest that the UCM treatments are better at modeling surface temperature during calm events driven by local circulations. In the wind fields, the spatial statistics indicate that treatments with a YSU PBL scheme may have a slight advantage, but the small sample size prevents a clear conclusion of which PBL scheme performs better.

c. *Radiosonde and Profiler Verification*

VTMX data from 3 rawinsonde sites and 3 radar wind profiler sites were used to verify the upper air fields (winds and temperature) of the four WRF forecasts for both IOPs. The main results from these comparisons are illustrated with selected plots below.

The performance of the four WRF runs in simulating the wind field during IOP 7 is illustrated in Fig. 18, which shows differences between simulated and observed (NIMA analyzed) wind speeds at station VX070, and Fig. 19, which

shows observed and simulated wind vectors at the nearby radiosonde location VX080. It is evident that all WRF runs overpredict the strength of the southerly flow in the lowest 2 km in the nighttime hours (05-12 UTC on Oct 18), while they all faithfully reproduce the observed wind shift above that level.

For IOP10, there are some persistent errors evident at VX070 (Fig. 20), most notably a positive wind speed bias at and above 3 km, and a smaller positive bias in the lowest 700 m. Evolution of the wind vectors at station VX010 (at the south end of the valley, Fig. 21), shows that the major features of the wind field evolution is captured fairly well by all WRF simulations.

Temperature and potential temperature profiles for VX080 during IOP 7 are shown in Fig. 22 and Fig. 23, respectively. As seen in both the temperature and potential temperature figures there is a very sharp nocturnal surface inversion early on Oct 17 and early on Oct 18. This feature is not fully resolved in any of the WRF runs, but the temperature profiles of the UCM runs are closer to the observed profiles, with a sharper curvature in the temperature profile, partly due to more accurate near-surface temperatures. In some cases the nocturnal surface temperature is at least 5 °C cooler than the non-UCM treatment. The timing of the erosion and reforming of the nocturnal surface inversion is evident in the corresponding potential temperature profiles in Fig. 23. Both the observations and the UCM runs show the nocturnal inversion forming around 00 UTC on Oct 18, while in the non-UCM this is delayed until around 03 UTC on Oct 18, a full 3 hours later. It is also notable that PBL heights during the heat of the day in non-UCM forecasts are too deep compared to observations. Without the urban parameterization, the WRF surface temperatures are too warm and result in a boundary layers that are too deep. This indicates that the UCM is crucial to accurately modelling the surface temperature and boundary layer, both day and night, during IOP 7.

Temperature and potential temperature profiles during IOP 10 at station VX010 (Fig. 24 and Fig. 25) show a much weaker nocturnal surface inversion, and the difference between the UCM and non-UCM treatments is almost indiscernible. Here the choice of PBL scheme exerts a larger influence, with slightly better agreement with observations for the runs with the Turb PBL scheme (MYJ).

4. Discussion and Conclusions

In the study reported here, we created WRF simulations for two Intensive Observing Periods (IOPs) during VTMX 2000 to evaluate the performance of parameterizations of the planetary boundary layer (PBL) and an urban canopy model (UCM). To accommodate the UCM, new landuse definitions were used for urban areas define the density of buildings in a variety of urban and suburban areas more precisely. The results reported here show that for urban locations, there was a clear benefit from parameterizing the urban canopy for simulation of the PBL and near surface conditions, particularly for temperature evolution at night. Using the UCM, the boundary layer collapses more quickly just after sundown than without an urban parameterization and closer to the observed timing. Near surface nighttime temperatures are also cooler when using the UCM, by as much as 5°C and are also in better agreement with observations. These improvements are most notable during quiet synoptic conditions (IOP 7) when flow was driven by local circulations. But the UCM created little to no improvement during the more active periods with synoptically driven flow.

Differences between PBL schemes were more significant outside of urban areas, but neither the eddy diffusivity scheme (YSU) nor the TKE scheme of vertical mixing (MYJ) produced consistently better results. Differences in the wind fields, whether attributable to different parameterizations of the boundary layer or urban

environments, were mostly transient features that moved and evolved with the flow. Comparison of WRF forecasts with upper air data, including temperature and wind profiles from the VTMX field campaign, showed virtually identical errors for all runs.

Our results, particularly the comparison of WRF vertical wind profiles to VTMX wind profiles, confirm the findings of (Zhong and Fast 2003) , that high-resolution mesoscale models are capable of reproducing local and mesoscale circulations. The implications for modeling the transport and dispersion of CO_2 suggest the need to take advantage of high resolution meteorological models and a parameterization of the urban environment. Future work will evaluate the effects of an urban parameterization in the meteorological fields on dispersion models. Given the improved simulation of surface temperature that an urban parameterization seems to produce, the effect on transport and dispersion modelling should be positive.

Acknowledgement The authors benefited from numerous interactions with Steve Wofsy and Kathryn McKain (Harvard University) in the planning and interpretation of these runs. We are grateful to Jerome Fast (Pacific Northwest National Laboratory) for providing us with VTMX2000 data, and to John Horel (University of Utah) for providing us with surface station data. Shawn Milrad (University of Kansas) performed an initial analysis of the data. Gridded analysis fields were obtained from the NARR website. We gratefully acknowledge help provided by John Halley Gotway of the WRF-MET team at NCAR in setting up and adapting WRF-MET. Funding was provided by Scitor Corporation, and supercomputing time was provided by NASA Ames.

References

Bowman, C., 2009: Moving from MM5 to WRF: what does it mean? *2009 Regional Smoke Meeting*, EPA, Spokane, WA, available from http://yosemite.epa.gov/R10/airpage.nsf/smoke/09+meeting.

Chen, F., H. Kusaka, R. Bornstein, J. Chine, C. S. B. Grimmond, S. Grossman-Clarke, T. Loridan, K. W. Manning, A. Martilli, S. Miao, D. Sailor, F. P. Salamanca, H. Taha, M. Tewari, X. Wang, A. A. Wyszogrodzki, and C. Zhang, 2010: The integrated WRF/urban modeling system: Development, evaluation, and applications to urban environmental problems. *Int. J. Climatol.*, early release, doi:10.1002/joc.2158.

Chin, H.-N. S., M. J. Leach, G. A. Sugiyama, J. M. L. Jr., H. Walker, J. S. Nasstrom, and M. Brown, 2005: Evaluation of an urban canopy paramterization in a mesoscale model using VTMX and URBAN 2000 data. *Mon. Wea. Rev.*, **133 (7)**, 2043–2068.

Doran, J. C., J. D. Fast, and J. Horel, 2002: The VTMX 2000 campaign. *Bull. Amer. Meteor. Soc.*, **83 (4)**, 537–551.

Gurney, K. R., D. L. Mendoza, Y. Zhou, M. L. Fischer, C. C. Miller, S. Geethakumar, and S. de la Rue du Can, 2009: High resolution fossil fuel combustion CO_2 emission fluxes for the United States. *Environmental Science & Technology*, **43 (14)**, 5535– 5541, 10.1021/es900806c.

Holt, T. and J. Pullen, 2007: Urban canopy modeling of the New York City metropolitan area: A comparison and validation of single- and multilayer parameterizations. *Mon. Wea. Rev.*, **135 (5)**, 1906–1930.

Hu, X.-M., J. W. Nielsen-Gammon, and F. Zhang, 2010: Evaluation of three planetary boundary layer schemes in the WRF

model. *J. Appl. Meteor.*, early release, doi: 10.1175/2010JAMC2432.1.

Lin, J. C., C. Gerbig, S. C. Wofsy, A. E. Andrews, B. C. Daube, K. J. Davis, and A. Grainger, 2003: A near-field tool for simulating the upstream influence of atmospheric observations: The stochastic time-inverted Lagrangian transport model (STILT). *J. Geophys. Res.*, **108 (D16)**, 4493, 10.1029/2002JD003161.

Nehrkorn, T., J. Eluszkiewicz, S. C. Wofsy, J. C. Lin, C. Gerbig, M. Longo, and S. Freitas, 2010: Coupled weather research and forecasting – stochastic time-inverted lagrangian transport (WRF-STILT) model. *Meteor. Atmos. Phys.*, **107 (1-2)**, 51–64, doi:10.1007/s00703-010-0068-x.

Otkin, J. A. and T. J. Greenwald, 2008: Comparison of WRF model-simulated and MODIS-derived cloud data. *Mon. Wea. Rev.*, **136 (6)**, 1957–1970.

Skamarock, W. C. and J. B. Klemp, 2008: A time-split nonhydrostatic atmospheric model for weather research and forecasting applications. *J. Comput. Phys.*, **227 (7)**, 3465–3485.

Zhong, S. and J. Fast, 2003: An evaluation of the MM5, RAMS, and Meso-Eta models at subkilometer resolution using VTMX field campaign data in the Salt Lake Valley. *Mon. Wea. Rev.*, **131 (7)**, 1301–1322.

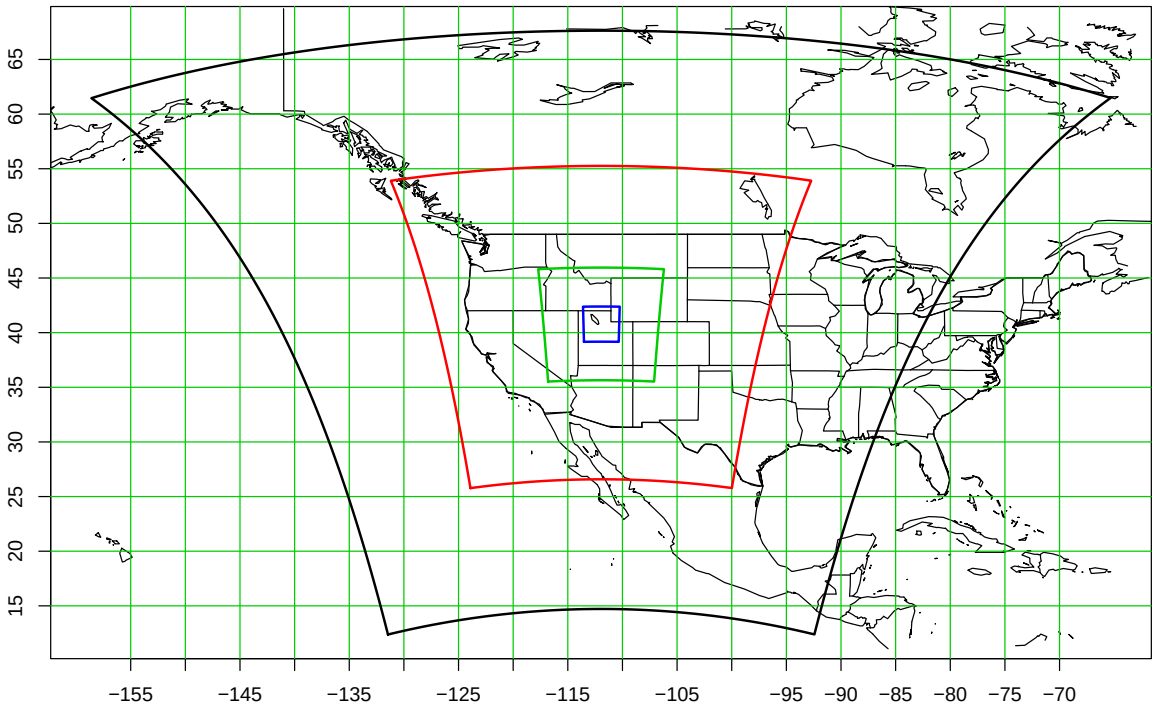

Figure 1: Outline of the 4 nested WRF model domains.

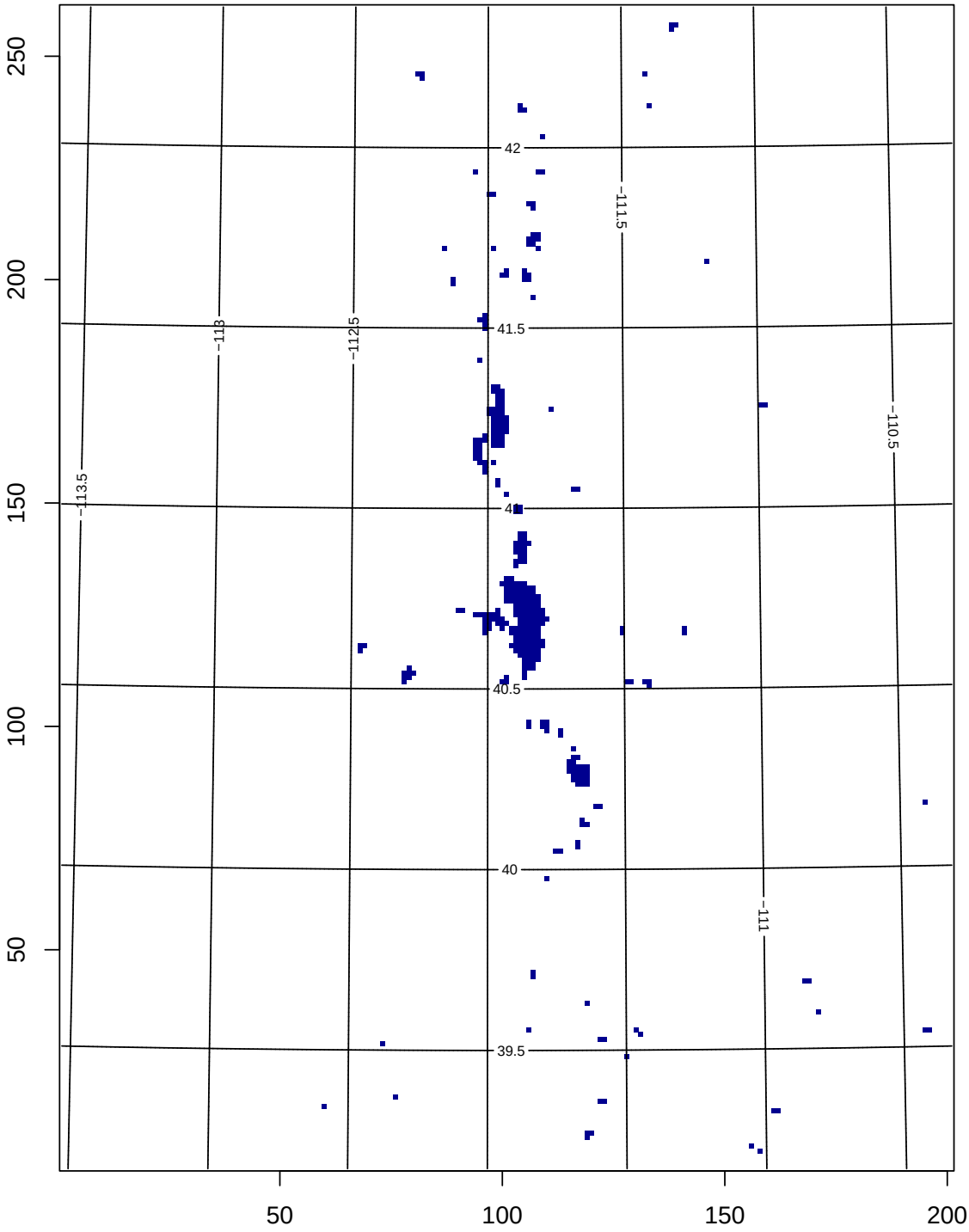

Figure 2: The single urban land use category (dark blue) of LU24 in the innermost domain, d04. LU24 is applied in the WRF runs with the UCM off.

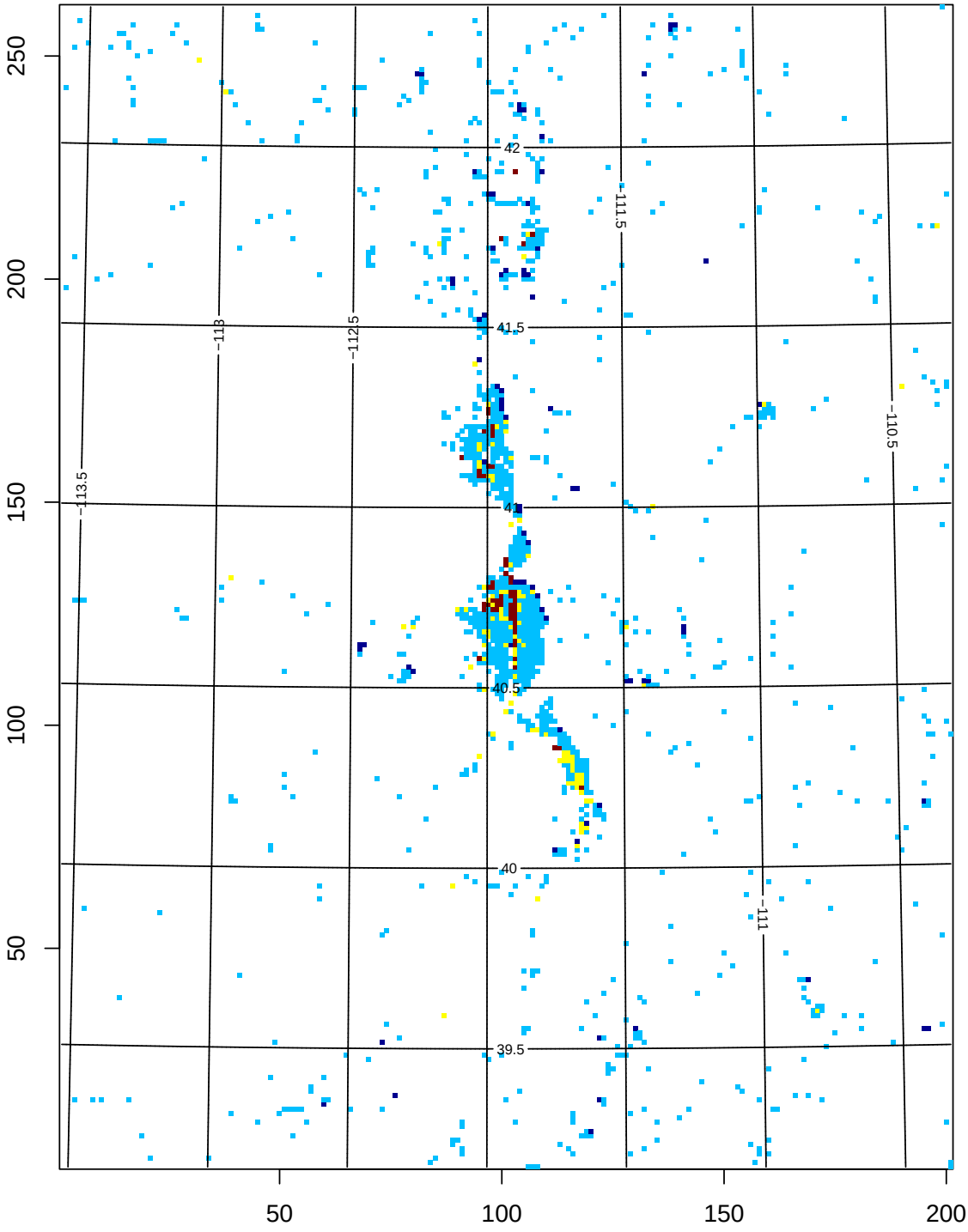

Figure 3: The urban land use categories of LU33 in the innermost domain, d04, where the three new categories (low intensity residential (light blue), high intensity residential (yellow), and industrial or commercial areas (dark red)) are overlaid on top of the single original category (dark blue) in Fig. 2. LU33 is applied in WRF runs with the UCM on.

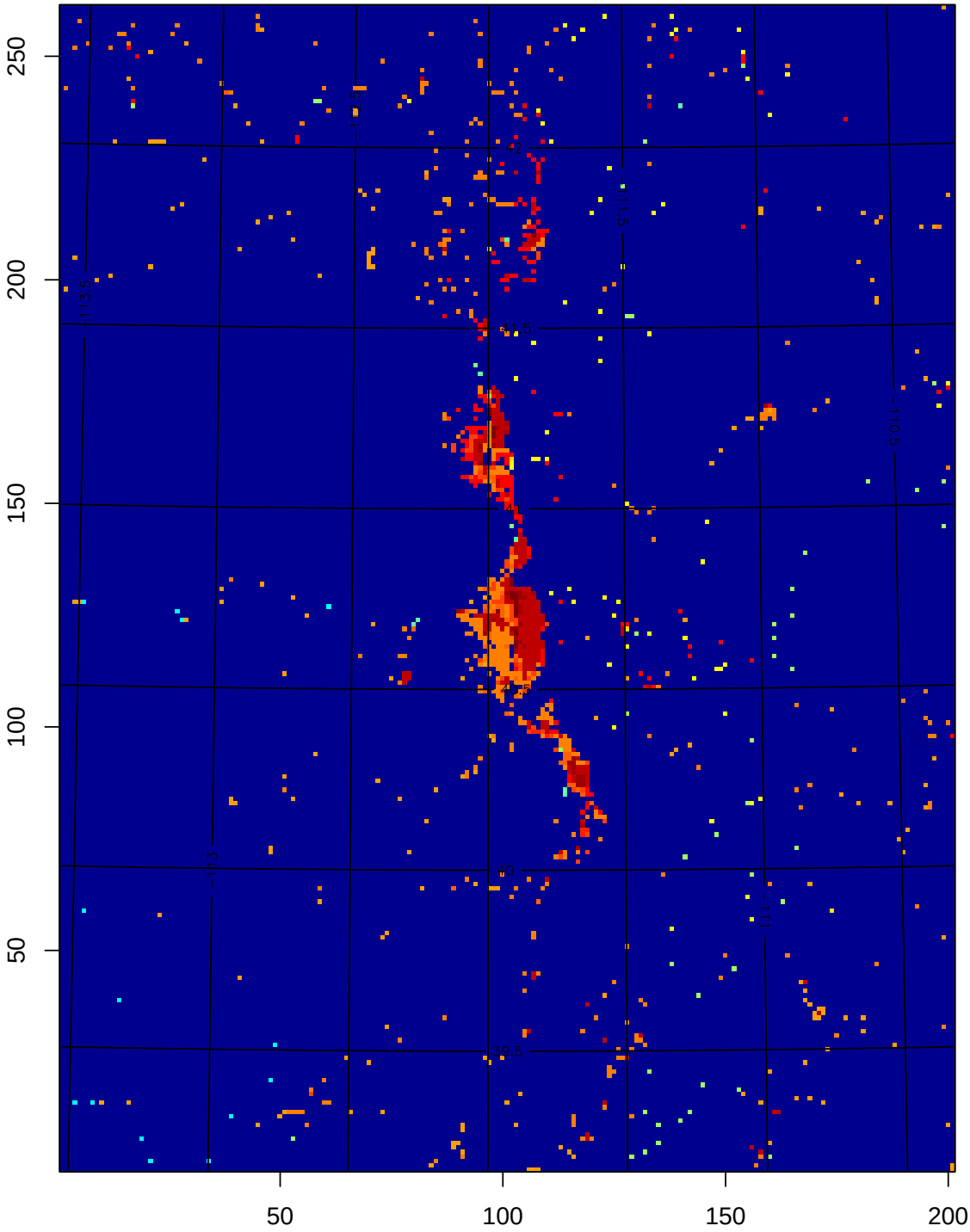

Figure 4: Difference map between the land use definitions in LU33 and LU24 for d04. The dark blue areas are where there has been no change in the land use definition between LU33 and LU24. The dark reds indicate areas where one of the three new urban categories overlaps the single urban category. The oranges and other colors indicate areas where the three new urban categories define urban areas that were previously not categorized as urban in LU24.

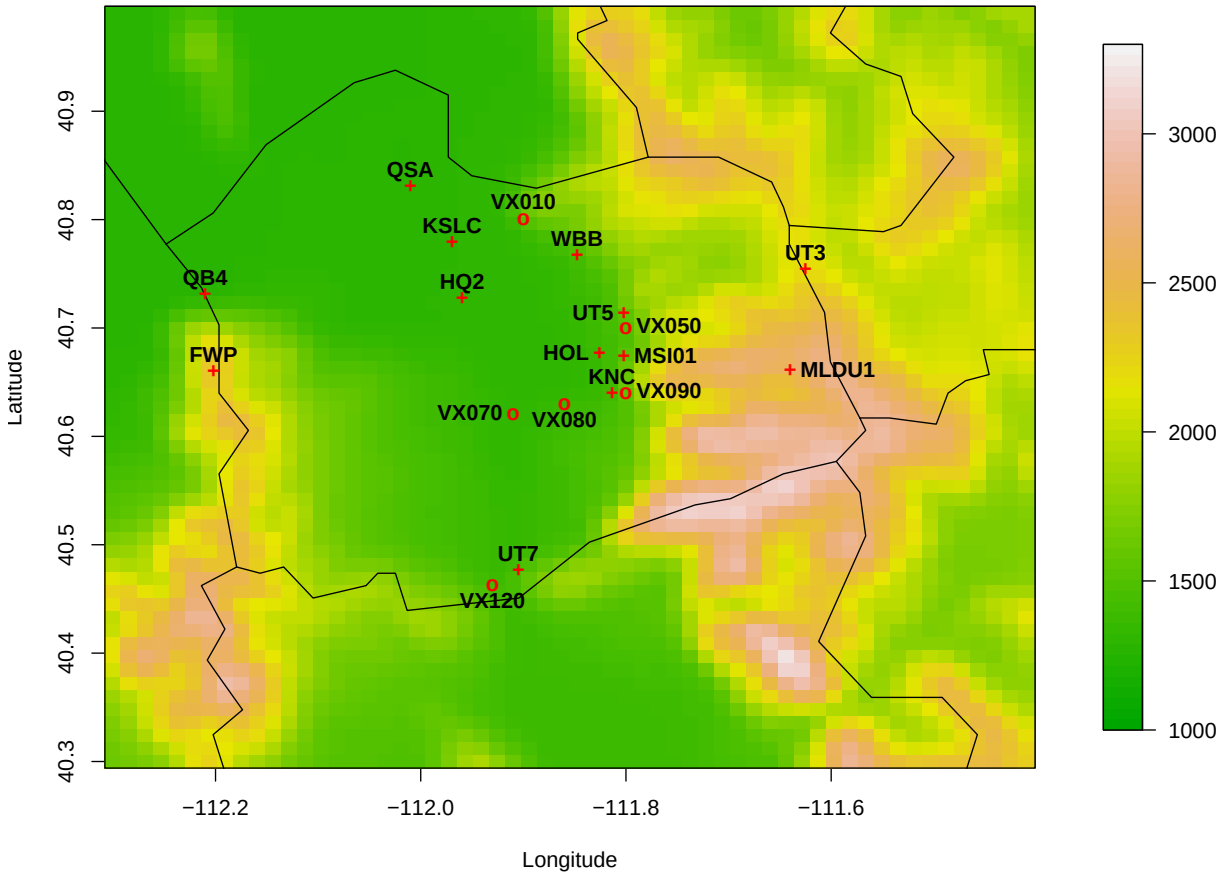

Figure 5: WRF terrain height map (meters above sea level) of the Salt Lake valley with VTMX upper air stations noted as circles and Mesowest surface stations noted as plus signs.

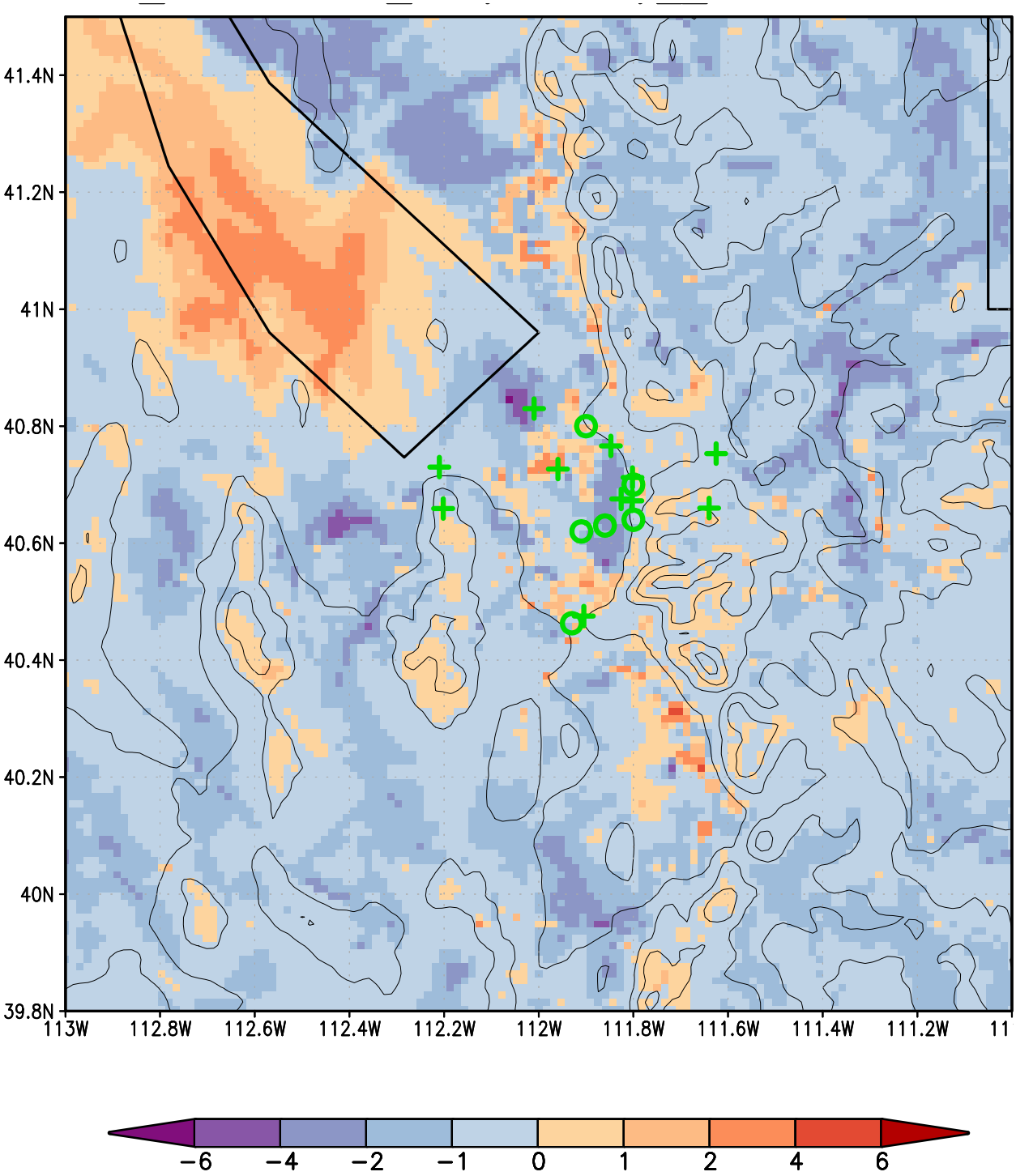

Figure 6: Two-meter temperature differences (° C) between the “Eddy” configurations, UCM minus no UCM, just before sunrise October 18th (1200 UTC). Terrain height is contoured in light gray every 500 m. As in Fig. 5, VTMX upper air stations are plotted as circles and Mesowest surface stations are plotted as plus signs.

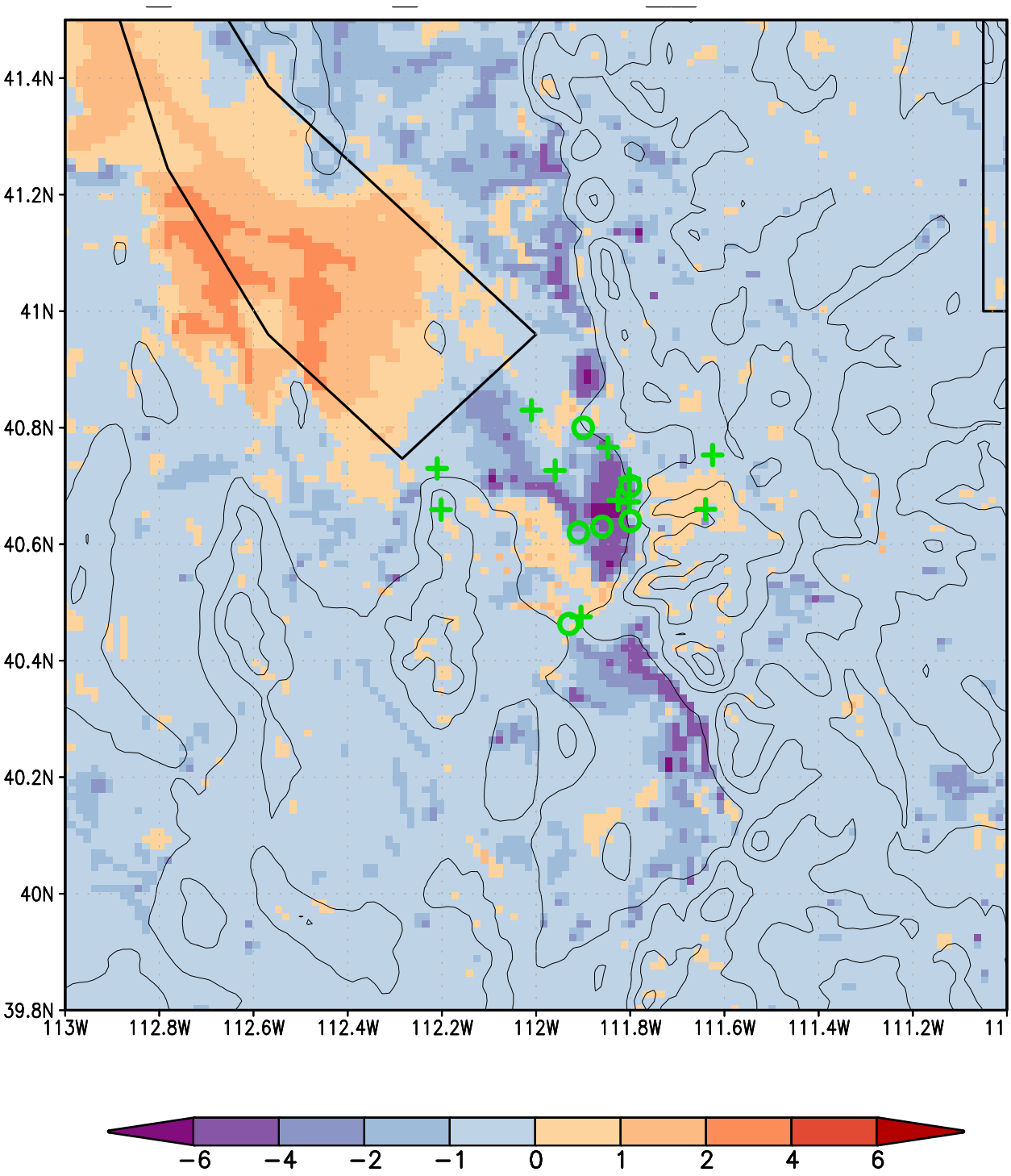

Figure 7: Same as Fig. 6 but for differences between the “Turb” configurations , UCM minus no UCM.

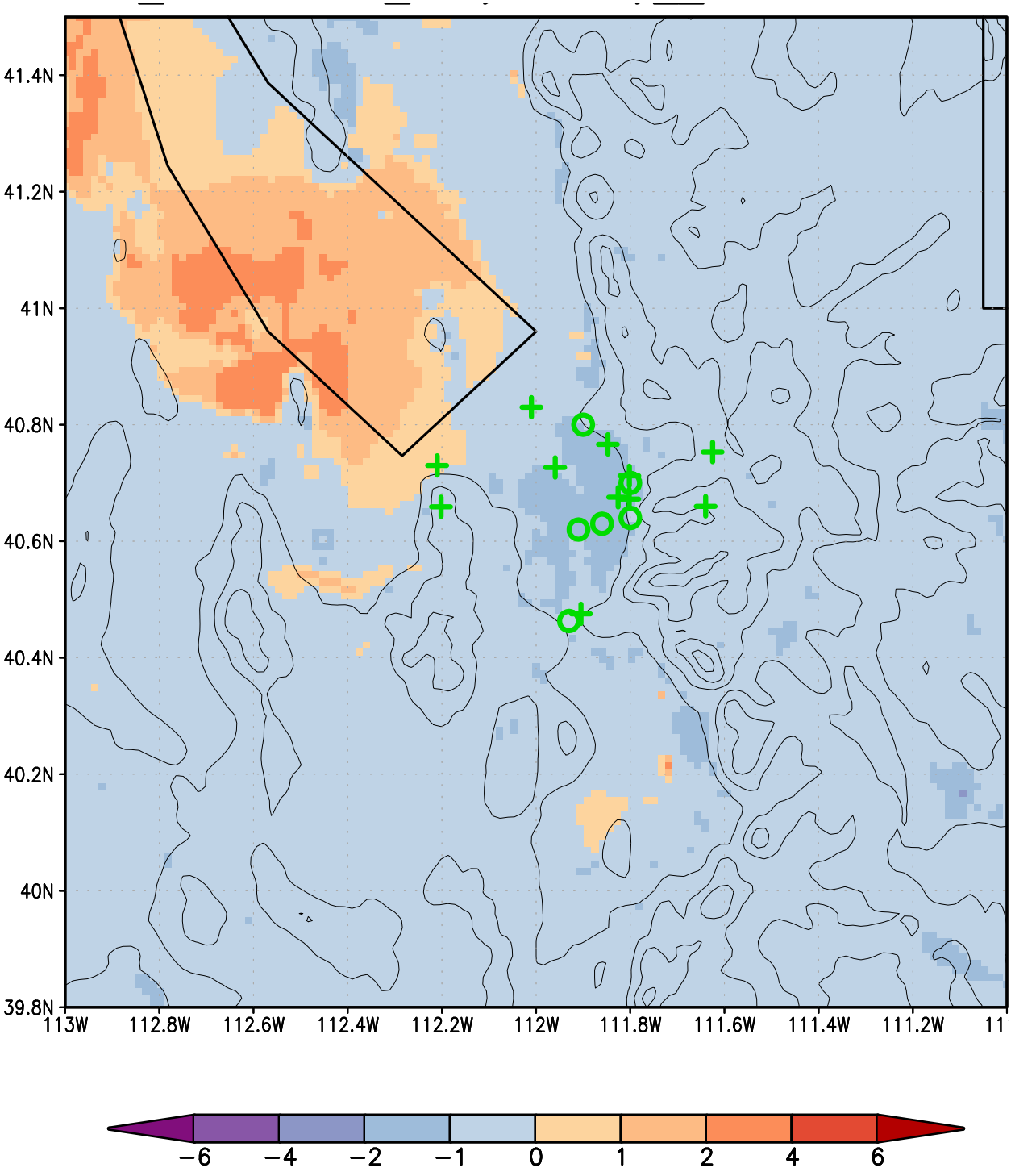

Figure 8: Same as Fig. 6 but valid near the end of daylight hours (2200 UTC) on October 18th.

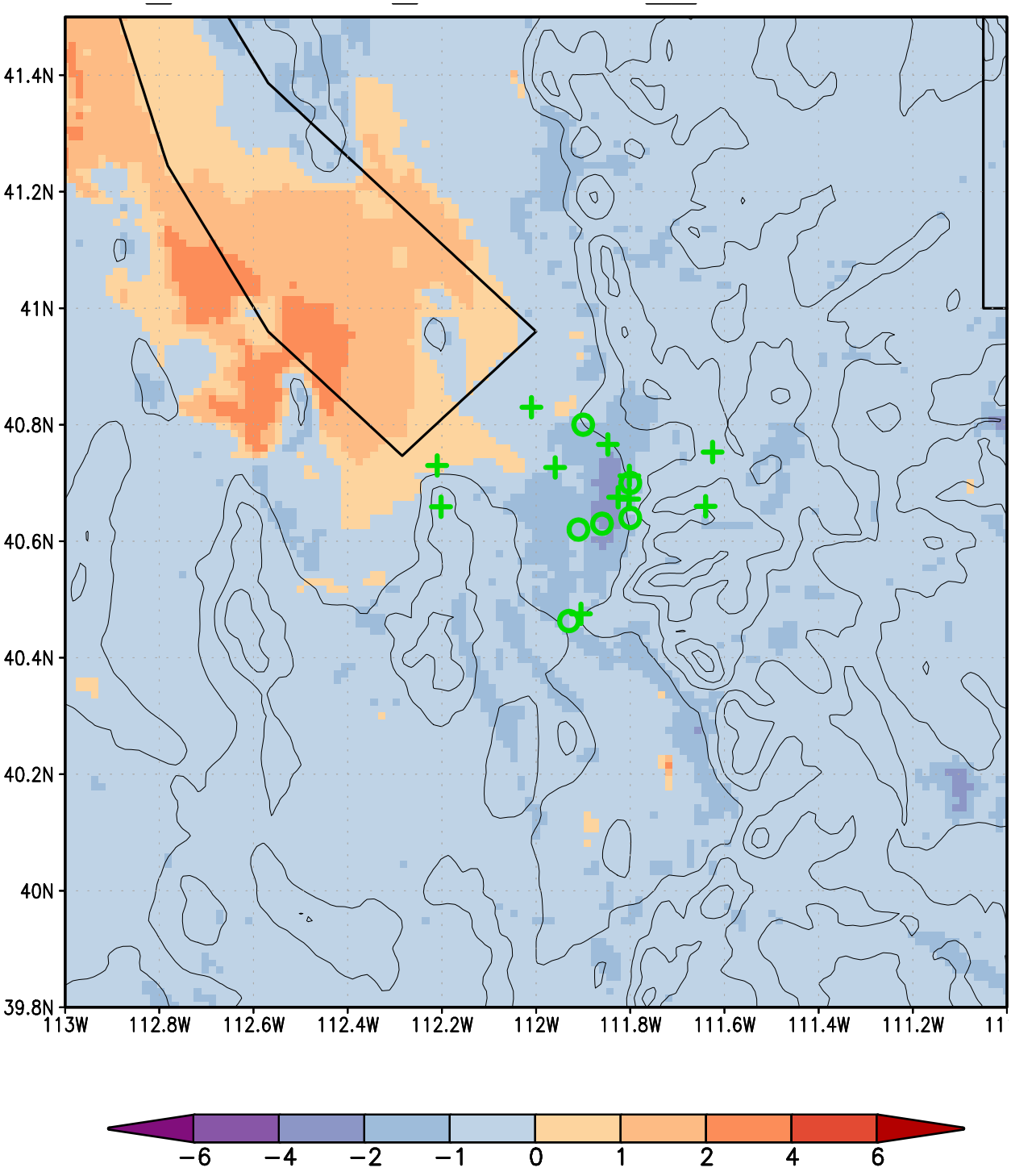

Figure 9: Same as Fig. 7 but valid near the end of daylight hours (2200 UTC) on October 18th.

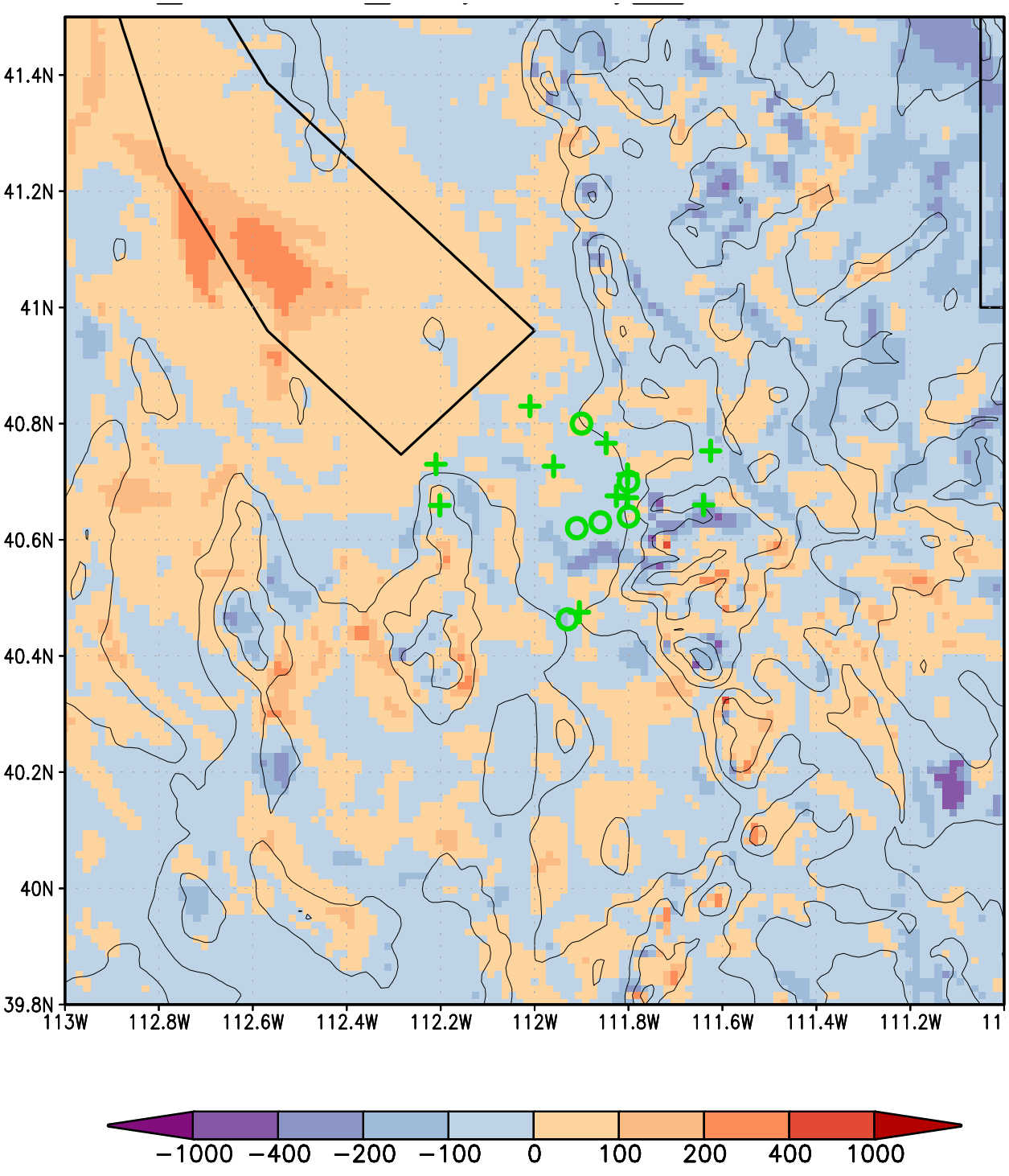

Figure 10: Typical PBL height differences for Eddy-U minus Eddy model configurations, valid 0400 UTC, October 19th, 2000.

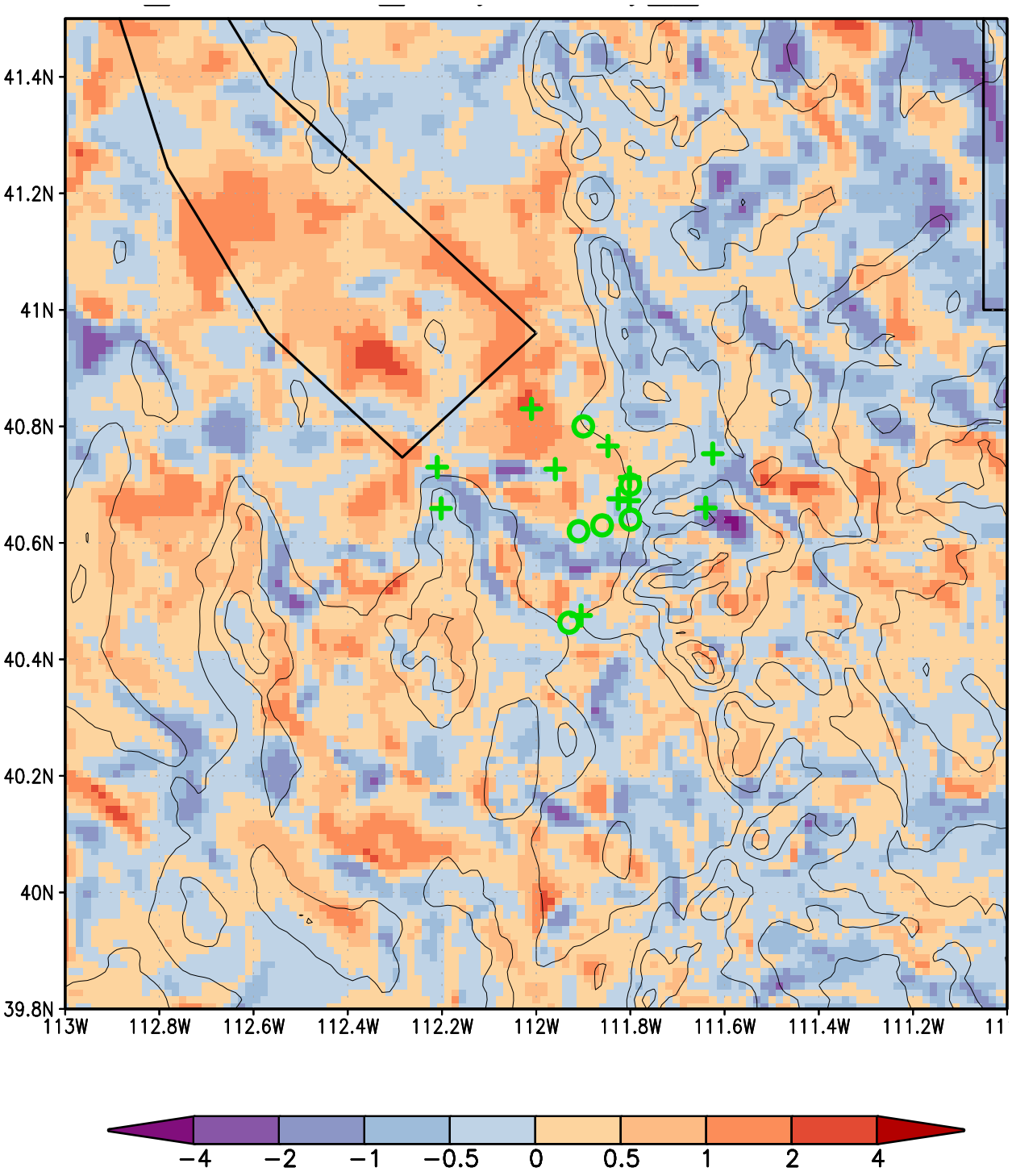

Figure 11: Typical 10 m wind speed differences for Eddy-U minus Eddy, valid 0400 UTC, October 19th, 2000.

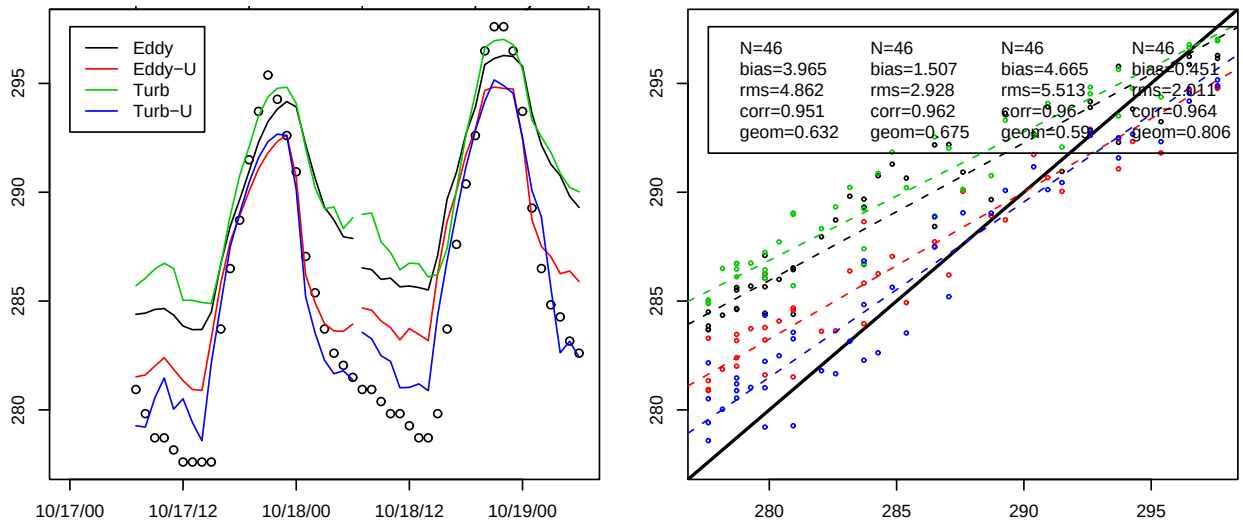

Figure 12: Time series of forecast and observed temperatures for station HOL for IOP7

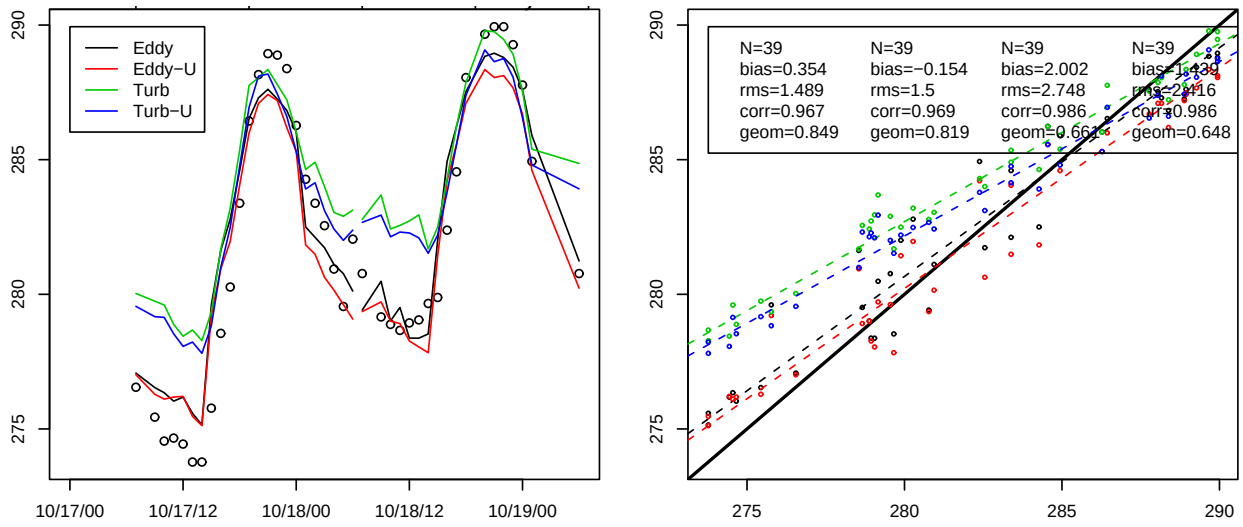

Figure 13: Time series of forecast and observed temperatures for station UT3 for IOP7

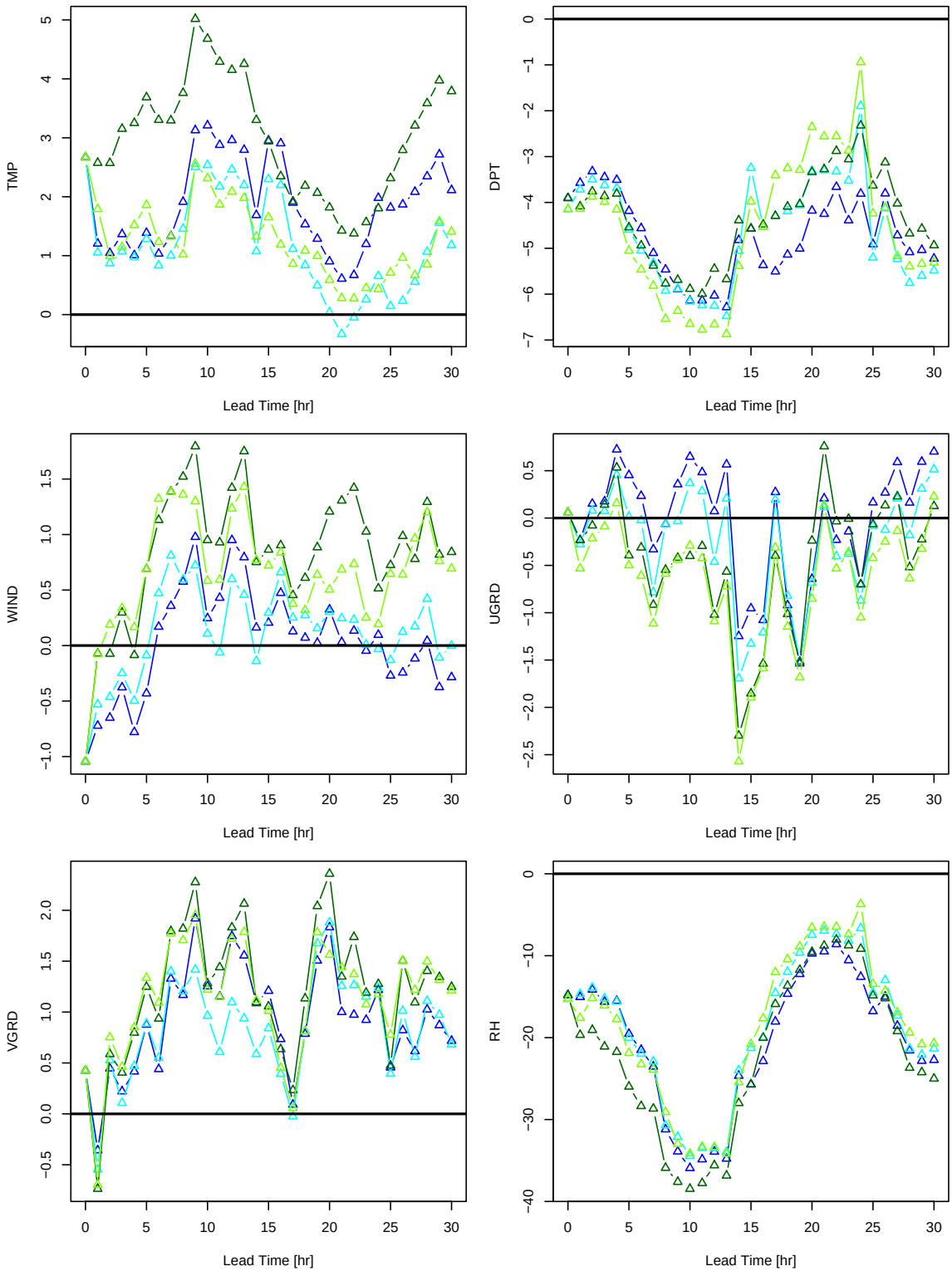

Figure 14: IOP 7 surface bias for strong QC MesoWest stations and each of the 4 treatments: Eddy (dark blue), Eddy-U (light blue), Turb (dark green), and Turb-U (light green).

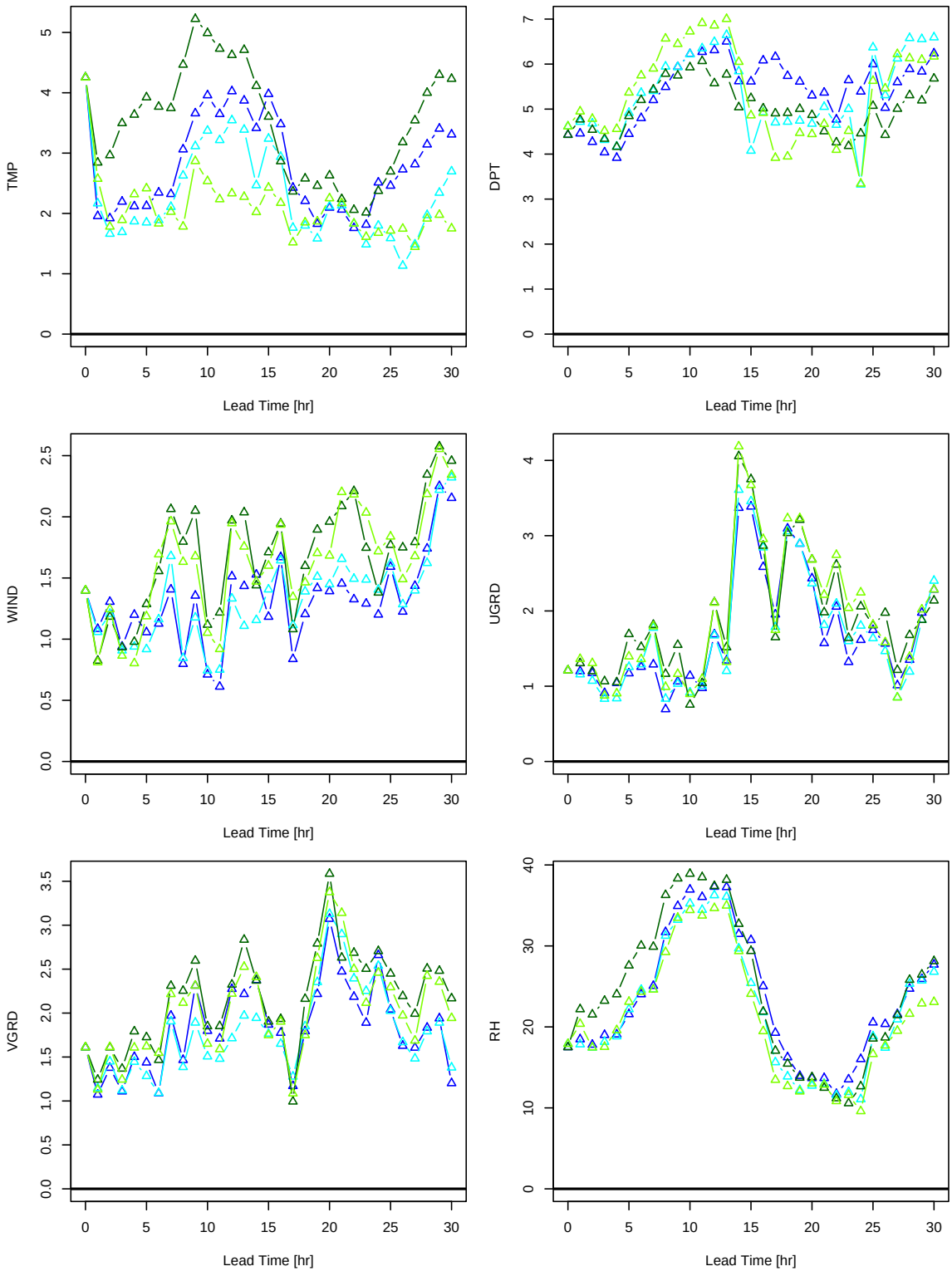

Figure 15: IOP 7 surface RMSE for strong QC MesoWest stations and each of the 4 treatments: Eddy (dark blue), Eddy-U (light blue), Turb (dark green), and Turb-U (light green).

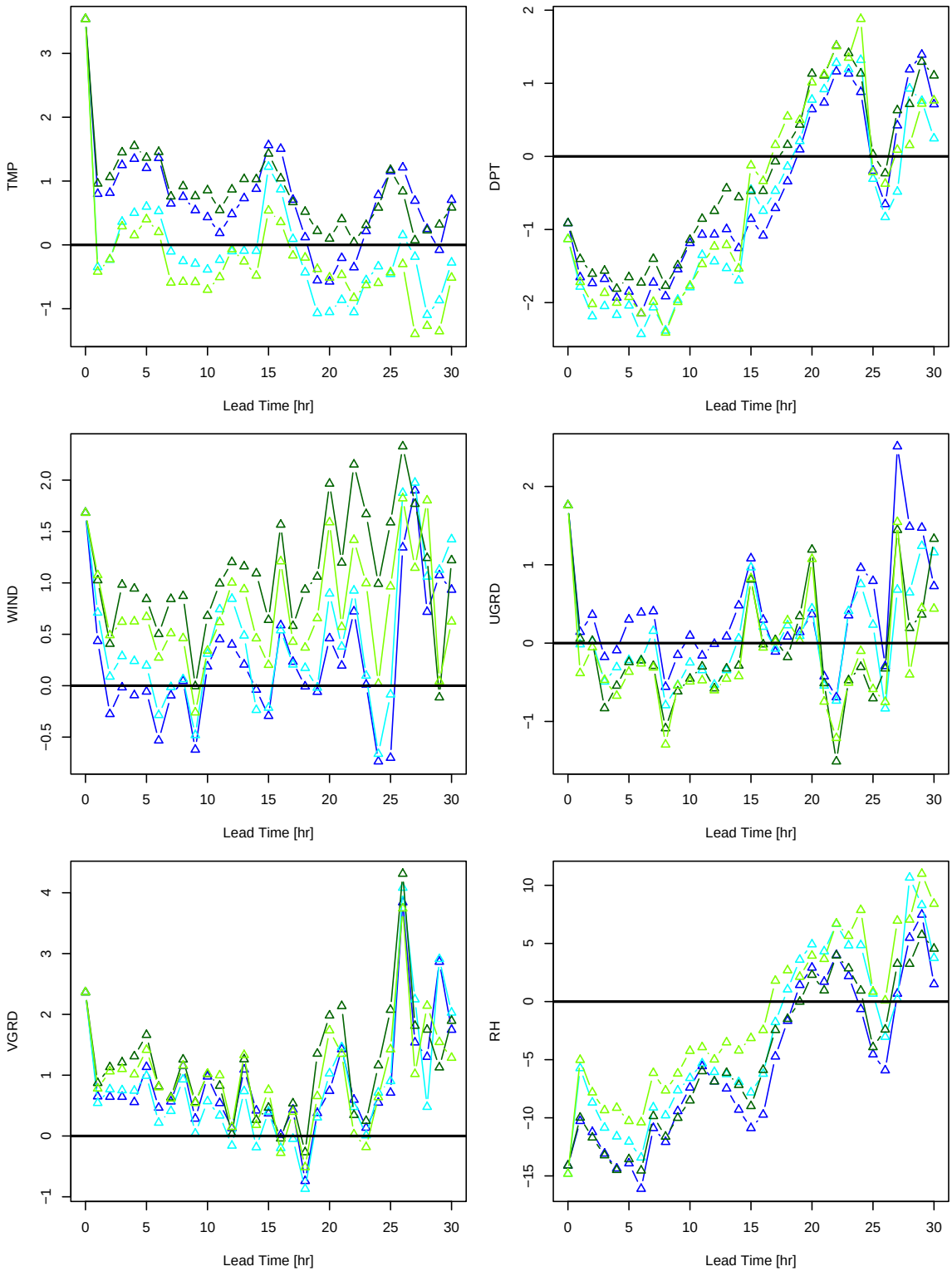

Figure 16: IOP 10 surface bias for strong QC MesoWest stations and each of the 4 treatments: Eddy (dark blue), Eddy-U (light blue), Turb (dark green), and Turb-U (light green).

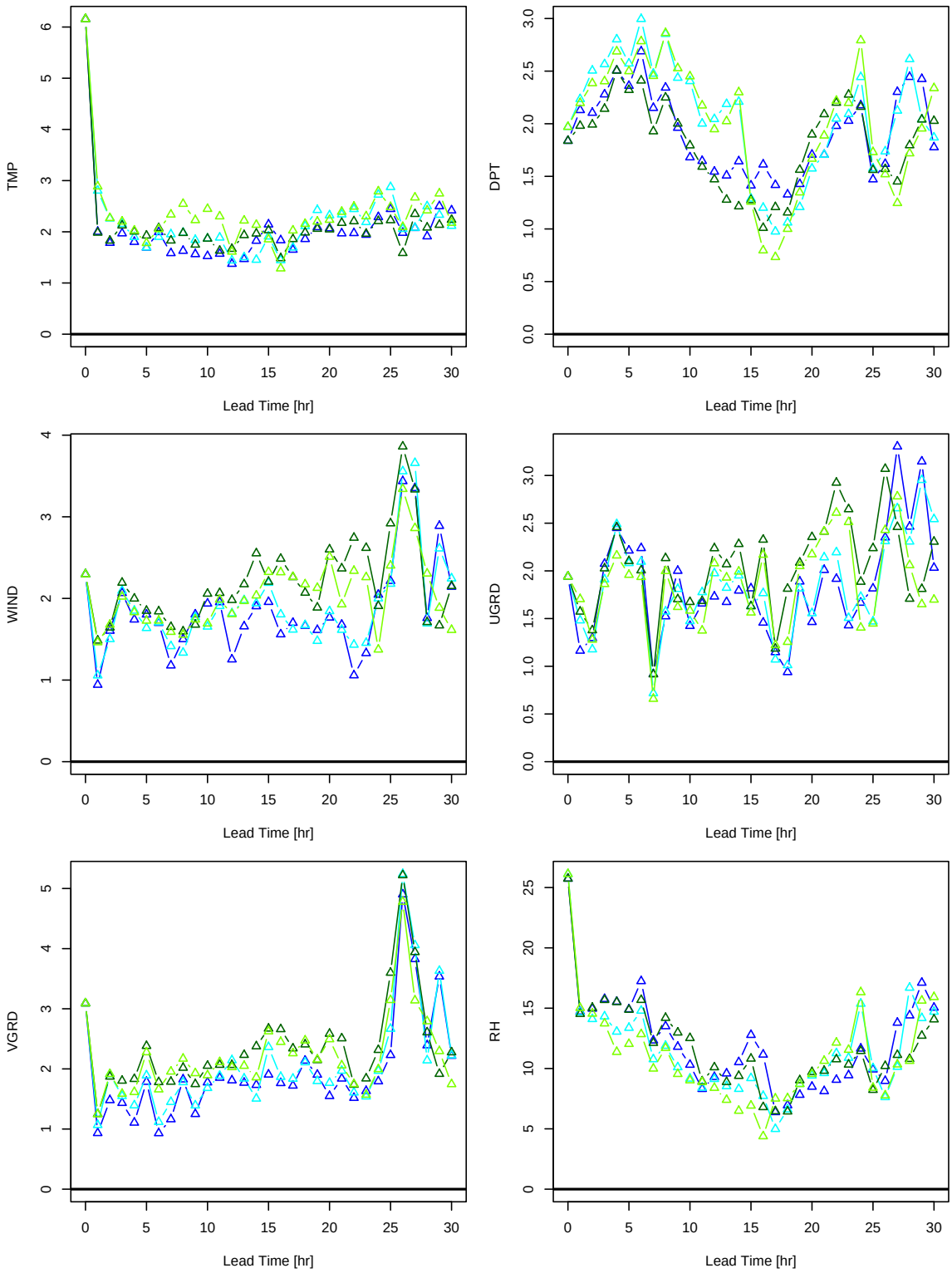

Figure 17: IOP 10 surface RMSE for strong QC MesoWest stations and each of the 4 treatments: Eddy (dark blue), Eddy-U (light blue), Turb (dark green), and Turb-U (light green).

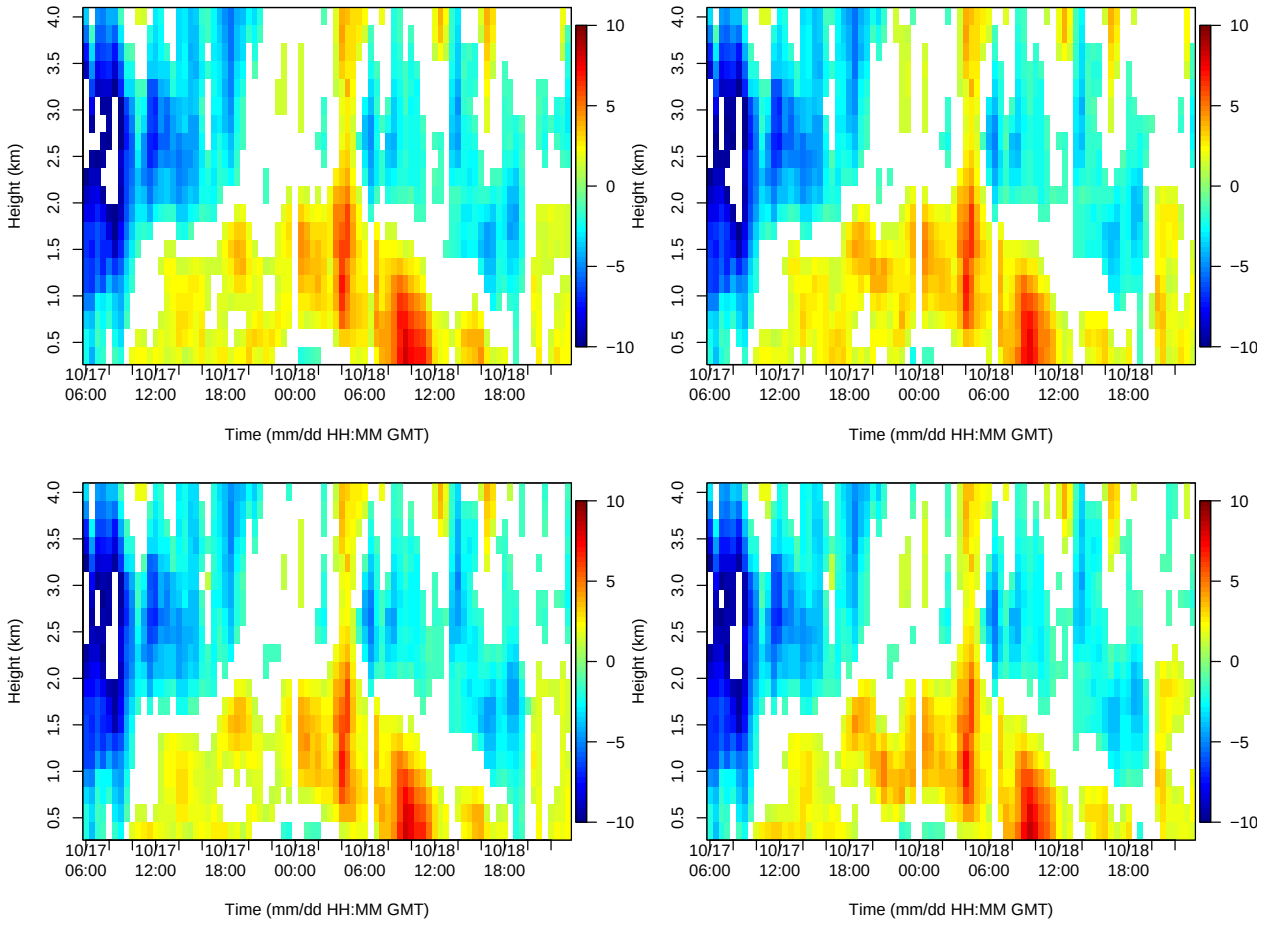

Figure 18: VX070, IOP 7 wind speed differences in m/s (forecast-obervations) in high mode where Eddy is upper-left, Eddy-U is bottom-left, Turb is upper-right, and Turb-U is bottom-right.

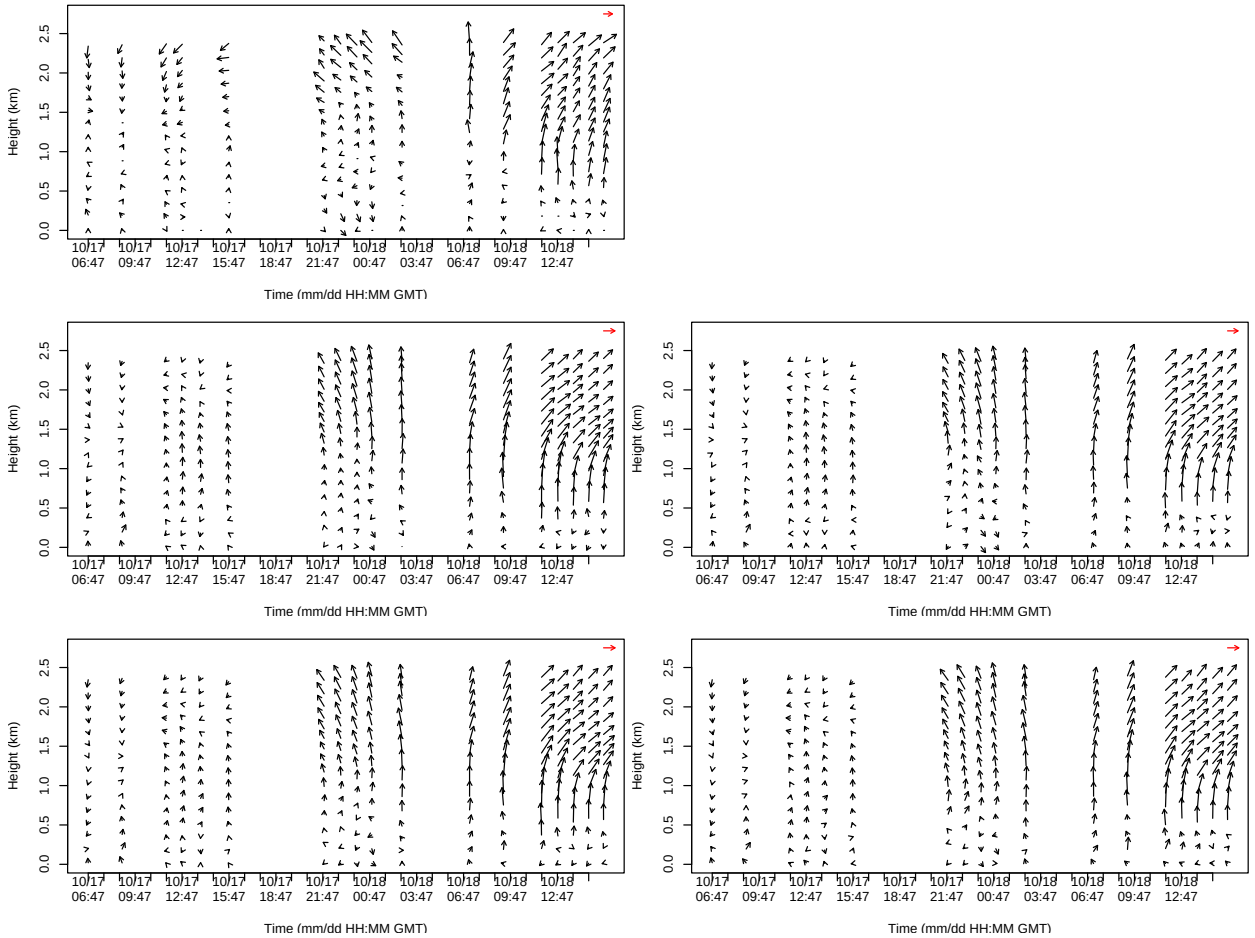

Figure 19: VX080, IOP 7 wind vector plot for observations in upper-left, Eddy in middle-left, Eddy-U in bottom-left, Turb in middle-right, and Turb-U in bottom-right. Red arrow denotes 5 m/s scale vector.

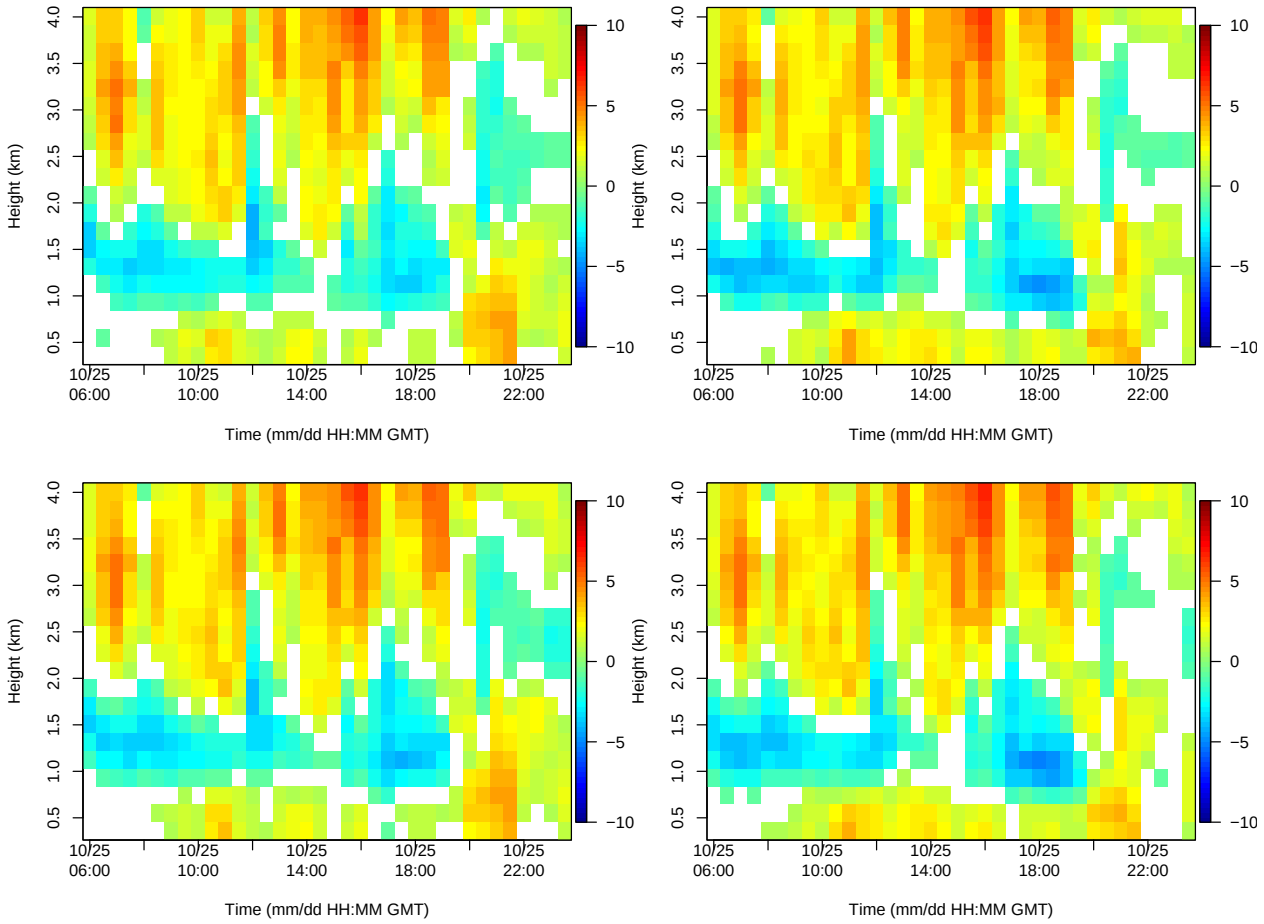

Figure 20: VX070, IOP 10 wind speed differences in m/s (forecast-observations) in high mode where Eddy is upper-left, Eddy-U is bottom-left, Turb is upper-right, and Turb-U is bottom-right.

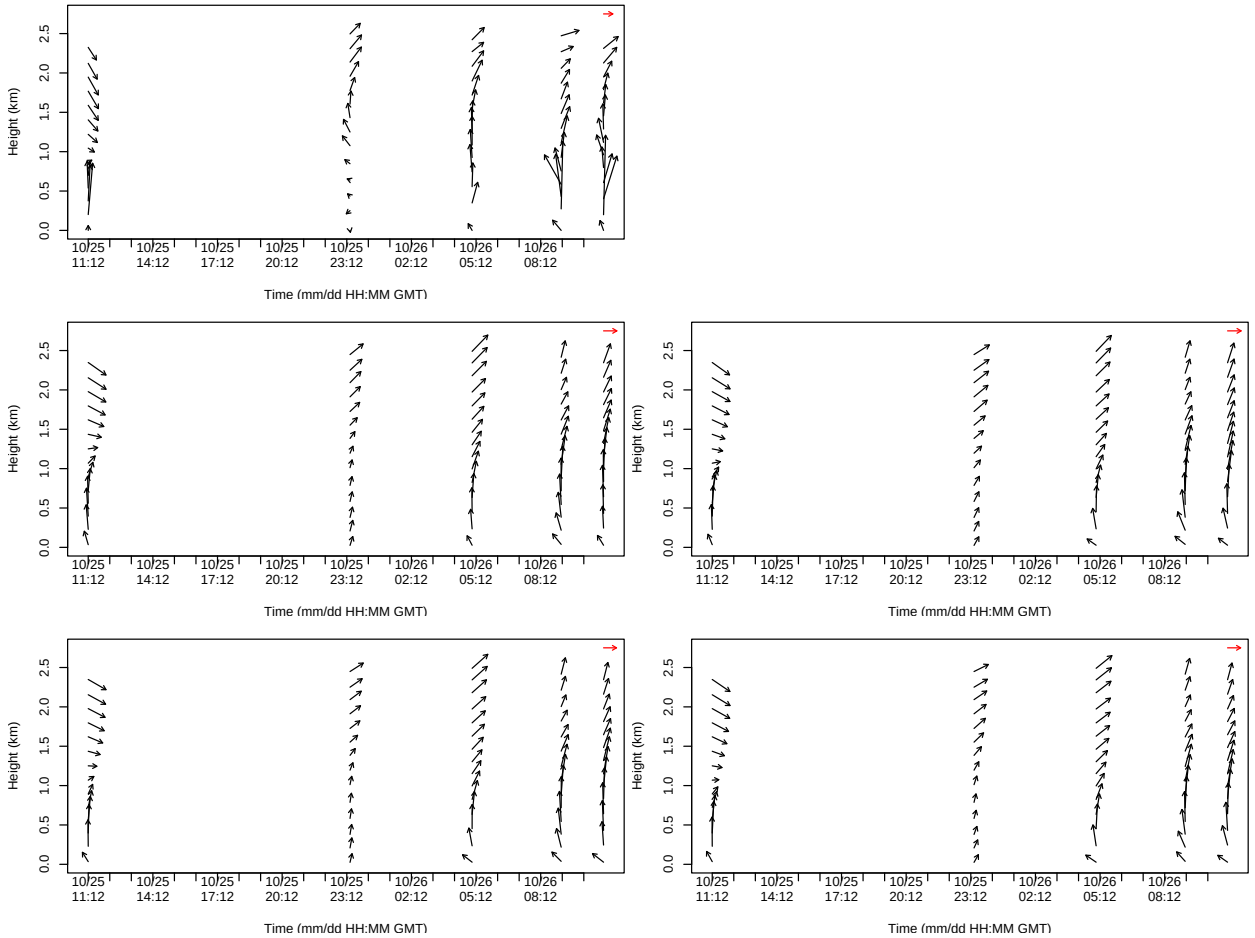

Figure 21: VX010, IOP 10 wind vector plot for observations in upper-left, Eddy in middle-left, Eddy-U in bottom-left, Turb in middle-right, and Turb-U in bottom-right. Red arrow denotes 5 m/s scale vector.

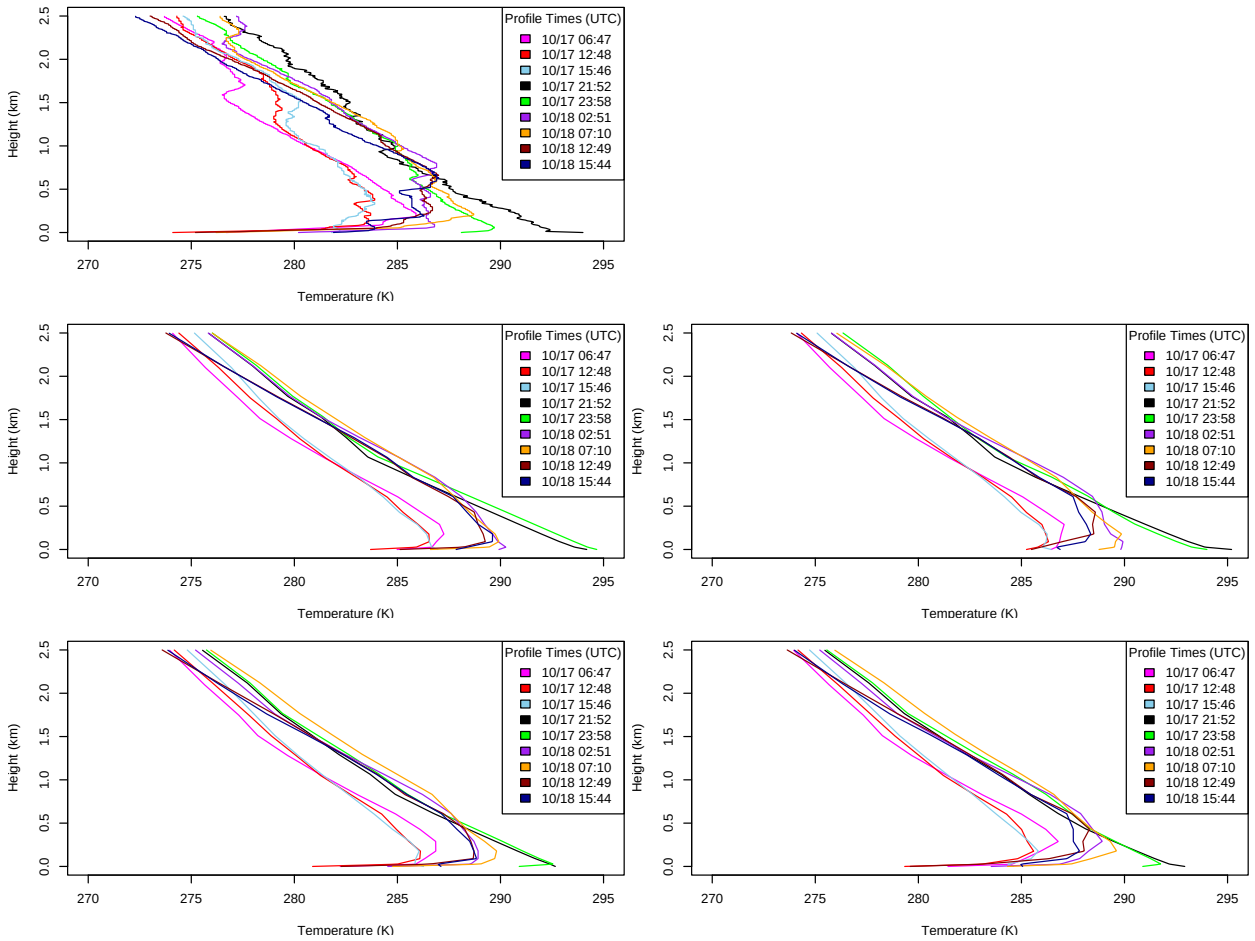

Figure 22: VX080, IOP 7 temperature profile plot at different sounding times for obervations in upper-left, Eddy in middle-left, Eddy-U in bottom-left, Turb in middle-right, and Turb-U in bottom-right.

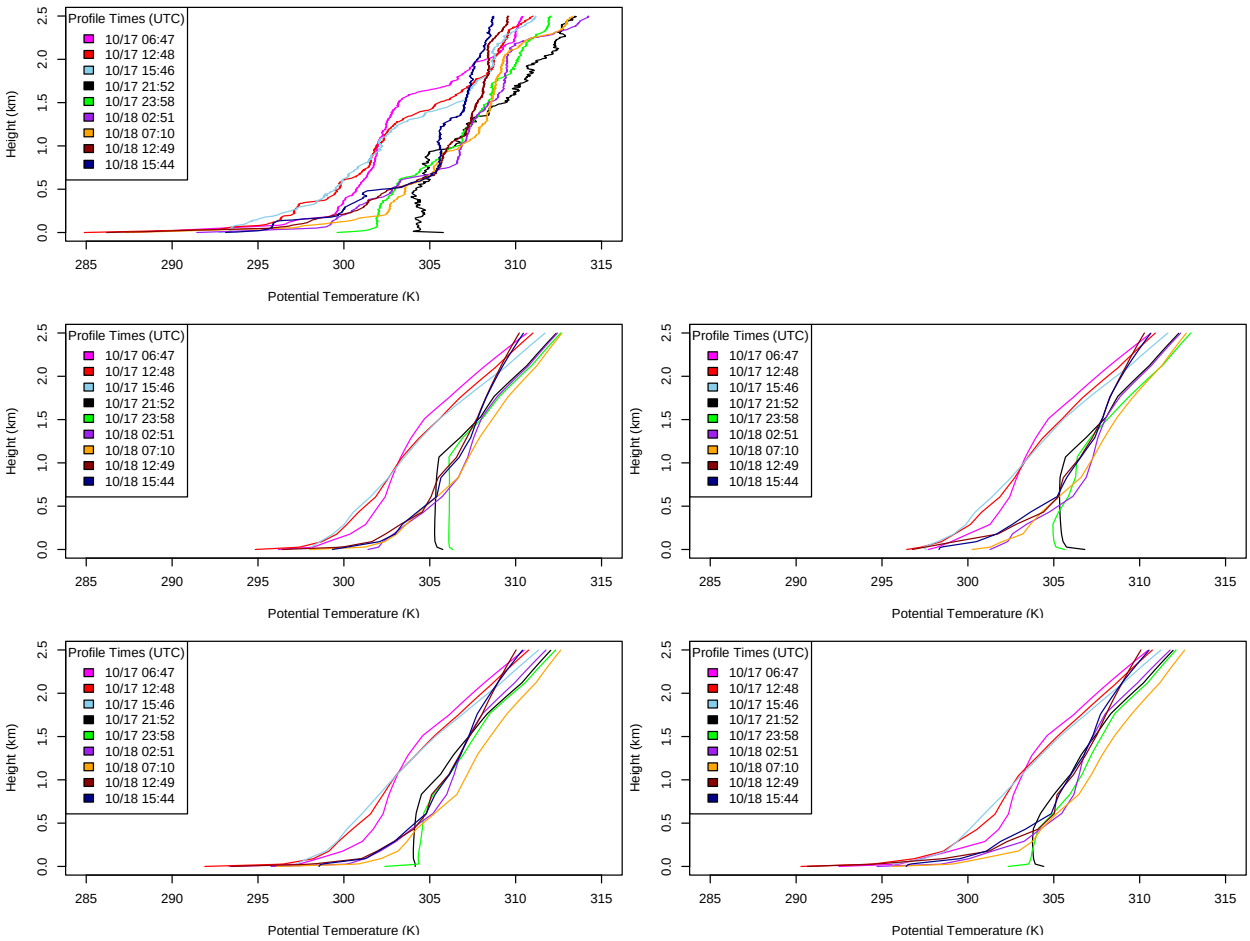

Figure 23: VX080, IOP 7 potential temperature profile plot at different sounding times for oberva-tions in upper-left, Eddy in middle-left, Eddy-U in bottom-left, Turb in middle-right, and Turb-U in bottom-right.

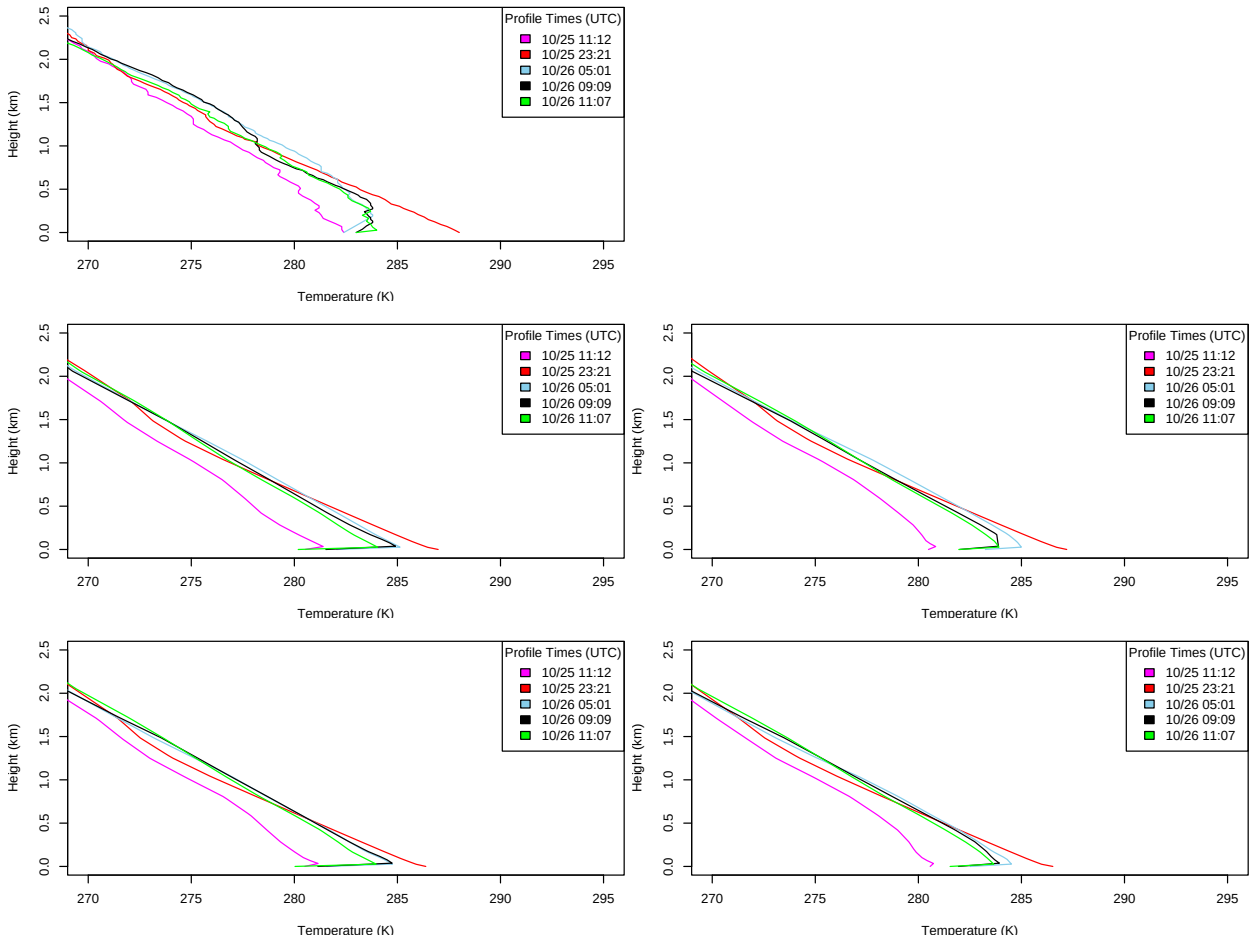

Figure 24: VX010, IOP 10 temperature profile plot at different sounding times for obervations in upper-left, Eddy in middle-left, Eddy-U in bottom-left, Turb in middle-right, and Turb-U in bottom-right.

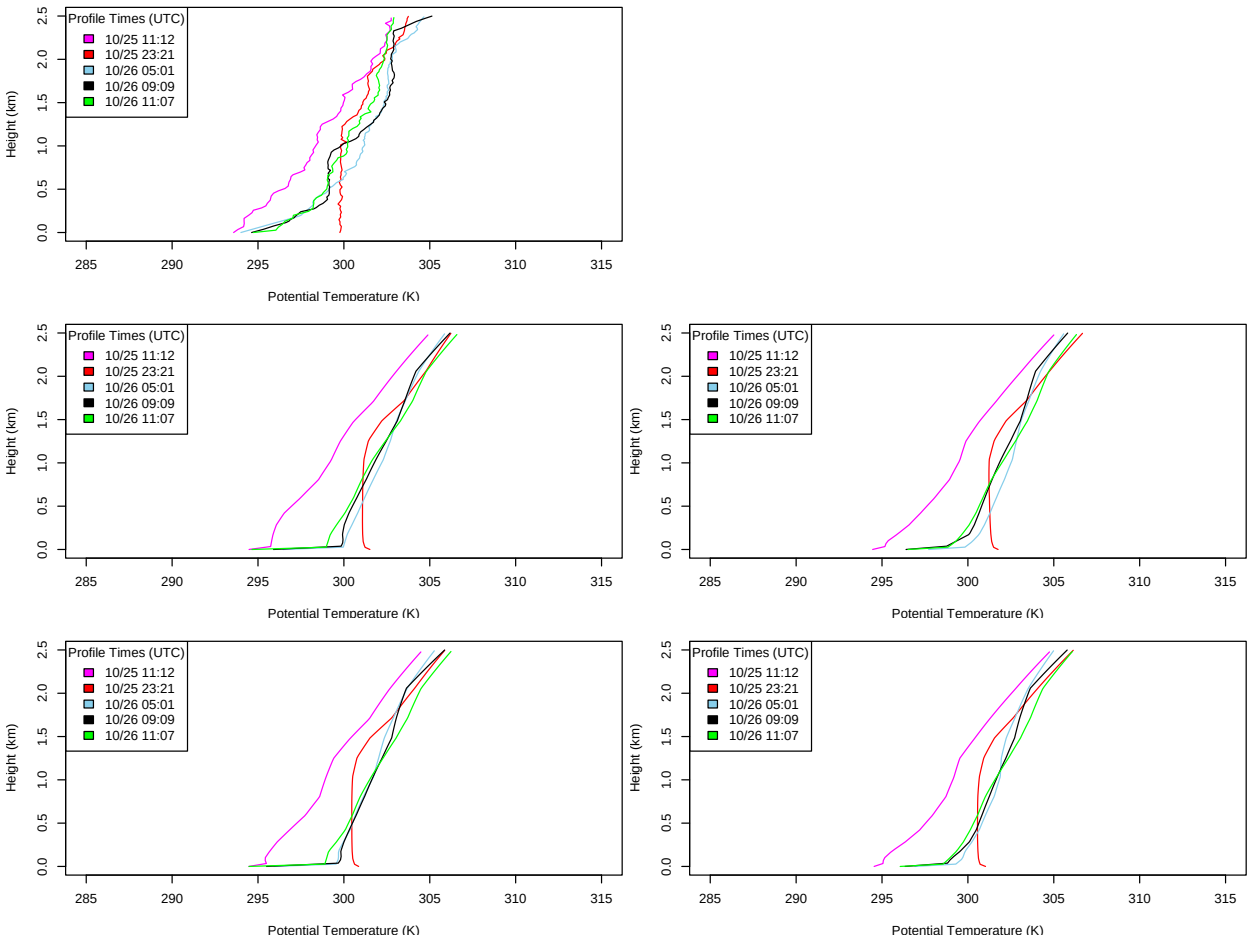

Figure 25: VX010, IOP 10 potential temperature profile plot at different sounding times for observations in upper-left, Eddy in middle-left, Eddy-U in bottom-left, Turb in middle-right, and Turb-U in bottom-right.

Table 1: Overview of WRF configuration common to all WRF runs.

Option	Description
Land Surface	Noah
LW radiation	RRTMG
SW radiation	RRTMG
Microphysics	Lin et al.
Convection	Grell-Devenyi (only domains d01-d02)
Nesting	Two-way, d01 (36km), d02 (12km), d03 (4km), d04 (1.33km)
Data Assimilation	Use analysis nudging in the outer grid only; perform 30-hour forecasts initialized every 24 hours (at 00 UTC), combine hours 7-30 from successive runs for a continuous time series of model fields
Nudging	Analysis; u,v,T,q at all levels above PBL, every 3 hours, 1 hour relaxation time
Time stepping	3rd order Runge-Kutta; 4 short time steps per long time step
Advection	5th order horizontal, 3rd order vertical positive definite advection for moisture and scalars
Diffusion	2nd order horizontal diffusion using Smagorinsky first-order closure
Damping	No upper level or vertical velocity damping; default values for divergence and external model damping

Table 2: WRF configuration of the sensitivity runs. See text for details

Name	PBL	Sfc Layer	Version	Urban Land-Use	UCM
Eddy	Yongsei University (YSU)	Monin-Obukhov	3.2	1	No
Eddy-U	Yongsei University (YSU)	Monin-Obukhov	3.2.1	3	Yes
Turb	Mellor-Yamada-Janjic (MYJ)	Monin-Obukhov (Janjic)	3.2	1	No
Turb-U	Mellor-Yamada-Janjic (MYJ)	Monin-Obukhov (Janjic)	3.2.1	3	Yes